Met.O.836

METEOROLOGICAL OFFICE

Scientific Paper No. 32

The Bushby-Timpson 10-level Model on a Fine Mesh

by G. R. R. BENWELL, M.A., A. J. GADD, Ph.D., J. F. KEERS, B.Sc., MARGARET S. TIMPSON, B.Sc. and P. W. WHITE, Ph.D.

LONDON: HER MAJESTY'S STATIONERY OFFICE

PRICE 11*s.* 0*d.* [55½p] NET

Met.O.836

METEOROLOGICAL OFFICE

Scientific Paper No. 32

The Bushby-Timpson 10-level Model on a Fine Mesh

by G. R. R. BENWELL, M.A., A. J. GADD, Ph.D., J. F. KEERS, B.Sc., MARGARET S. TIMPSON, B.Sc. and P. W. WHITE, Ph.D.

LONDON
HER MAJESTY'S STATIONERY OFFICE
1971

U.D.C. 551.509.313:
551.509.324.2

ISP

Contents

1. Summary 1
2. Introduction 1
3. System of equations 3
4. Finite-difference scheme 4
5. Initialization 6
6. Topography, friction and lateral diffusion . . . 20
7. Condensation and evaporation 32
8. Surface exchanges of sensible and latent heat . . . 35
9. Sub-grid-scale convection 40
10. An example of forecasts from the 10-level model . . 44

Bibliography 50

Appendix I 52

Appendix II 55

NOTATION

(Meaning of symbols used unless otherwise stated)

a	horizontal grid length at the North Pole (54·4473 km)
b	vertical grid length (100 mb)
c_p	specific heat of air at constant pressure
c_h, c_l, c_m	fractional cloud cover, high, low, medium
C_D, C_S, C_L	drag coefficient, general, sea, land
f	Coriolis parameter
F', F	fraction of solar radiation transmitted through clear atmosphere, cloudy atmosphere
F_G	flux of heat into the ground
F_H	flux of sensible heat at 1000-mb surface into the atmosphere
F_W	flux of water vapour at 1000-mb surface into the atmosphere
g	gravitational acceleration
h	height of pressure level
h'	thickness of 100-mb layer
H	topography, height of terrain
i, j, k	grid-point position indicators in the x, y, p directions (see also suffixes)
k_E	surface exchange coefficient for sensible heat and water vapour
$\mathbf{k}$	unit vertical vector
K	lateral diffusion coefficient
L	latent heat of condensation
L_0', L_0	net long-wave radiation at zero insolation for clear atmosphere, cloudy atmosphere
M_k	liquid water falling through level k per double time-step
m	map magnification factor, $=\sec^2(\pi/4-\phi/2)$, ϕ being the latitude
p	pressure
P_k	rate of rainfall at level k
Q	rate of non-adiabatic heating caused by condensation and evaporation, surface exchanges and small-scale convection
r	humidity mixing ratio
r_s	saturation mixing ratio
R_E	radius of earth
R	gas constant
R_N	net radiation flux at the ground
S	solar constant
T	temperature
t	time
u, v	horizontal wind components
V	wind speed
$\mathbf{V}$	horizontal wind vector
w	vertical velocity ($\equiv \mathrm{d}z/\mathrm{d}t$)
W	rate of change of humidity mixing ratio due to condensation and evaporation, surface exchanges, and small-scale convection
X	large-scale relative humidity

x, y	horizontal co-ordinates on a stereographic grid
z	height above ground
*	indicates smoothing
α	albedo of the land surface
β	a ground heating coefficient
γ	lapse rate
$\gamma_c, \gamma_d, \gamma_s$	lapse rate, neutral, dry adiabatic, saturated adiabatic
δ	solar declination
δt	time step
ϵ	a constant equal to the ratio of molecular weight of water to that of dry air (0.622)
ζ	vertical component of relative vorticity
ζ_a	vertical component of absolute vorticity
θ	solar angle
Θ	potential temperature
κ	$= R/c_p$
λ	longitude
μ	ratio of heat flux into ground to net radiation flux
ρ	density
τ	frictional stress
τ_X, τ_Y	components of frictional stress
ϕ	latitude
χ	velocity potential
ψ	stream function
ω	vertical component of motion ($\equiv \mathrm{d}p/\mathrm{d}t$)

SUFFIXES

x, y, p, t	partial differentiation with respect to space and time
i, j	horizontal position indicators
k	pressure-level indicator ($k = 1$ at 100 mb, $k = 10$ at 1000 mb)
$k+\frac{1}{2}$	layer indicator (between levels k and $k+1$)
100, 200 ... 1000	relate to particular pressure levels
150, 250 ... 950	relate to particular layers 100 mb thick, e.g. 150 relates to layer between 100 and 200 mb
0	denotes value at ground.

The Bushby-Timpson 10-level Model on a Fine Mesh

by G. R. R. Benwell, M.A., A. J. Gadd, Ph.D., J. F. Keers, B.Sc., Margaret S. Timpson, B.Sc. and P. W. White, Ph.D.

1. SUMMARY

A full description is given of the 10-level numerical model which has been developed over the past few years in the Forecasting Research Branch of the Meteorological Office as a basis for computations in investigating the dynamics of fronts and in predicting frontal rainfall. The basic model as originally proposed assumed that the atmosphere was frictionless and inviscid. It also assumed that there were no surface transfers through the bottom surface boundary of the atmosphere. No account was taken of physical effects such as forced ascent or descent in the vicinity of high ground or of motions smaller than those which could be resolved by the grid. The formulation now incorporates the effects of surface friction, topography, heat and moisture transfers across the bottom boundary, sub-grid-scale convection and lateral diffusion. Furthermore, the restriction that the initial wind fields should be non-divergent has been removed and vertical motions are present initially. However, no ice stage has yet been incorporated into the condensation physics.

The model is still undergoing development; this paper covers the stages of the development up to the end of 1969 and an example of a recent forecast is included.

2. INTRODUCTION

2.1. *General background*

All methods of numerical weather prediction are derived from the same general equations embodying the principles of conservation of momentum, mass and energy. These are the Newtonian equations of motion, the equation of continuity, and a thermodynamic energy equation. The basic first-order hydrodynamic and thermodynamic equations appropriate to an inviscid, hydrostatic atmosphere are usually referred to as the 'primitive equations' and, in the first attempt to predict the weather numerically, Richardson[1]* used an approach which was the straightforward application of finite-difference approximations to the primitive equations. Richardson's manually computed predictions were not successful, but interest in the subject was reawakened in the 1940s following the advent of high-speed electronic computers and the widespread adoption of radiosonde techniques for obtaining regular sampling of the atmosphere. At that time it appeared to be necessary to manipulate the equations so as to remove solutions of a non-meteorological character from the equations of motion, and this led to a second approach, favoured by Charney[2] and usually referred to as the vorticity approach. In this approach one of the first steps in obtaining the filtered equations is to derive the vertical component of vorticity and then eliminate the horizontal divergence by means of the equation of continuity. Essentially the result of using this approach is that solutions appropriate to sound and gravity waves are eliminated from the possible solutions of the general equations and therefore a considerably larger time-step can be used without violating the computational stability criteria (Courant, Friedrichs and Lewy[3]). A further advantage accruing from the vorticity approach is that since the geostrophic (or similar) assumption is made the winds and vorticity can

* Superscript figures refer to bibliography on p. 50.

always be computed directly from the grid-point values of the geopotential height fields and it is therefore unnecessary to store these variables.

The assumptions made in the vorticity approach and the horizontal resolution of about 300 km used in the current operational model are adequate for predicting the behaviour of the large atmospheric systems such as the semi-permanent anticyclones and deep depressions. However, the prediction of smaller-scale features associated with rain cannot be handled by the vorticity approach, even if a finer resolution is chosen, since the assumptions are no longer valid when applied to these smaller systems where, for example, ageostrophic motions are important. Therefore the primitive equation approach has to be used despite the inherent difficulties. Section 5 deals with the initial-data problems, such as the removal of static instability, and the assumptions made about the initial wind fields in order to ensure that there are no large, spurious divergences present initially in the horizontal motion field. Equally important is the need to prevent such divergences developing from the equations as the computation proceeds, especially at the lateral boundaries, and this aspect will be mentioned in Section 3. One further point, a direct result of the use of the primitive equations, is the need to use a very reduced time-step in order to control the fast-moving gravity waves. The use of a reduced grid length and a very short time-step means that a large, very fast computer must be employed. All the development of this model has so far been carried out on the Science Research Council Atlas computer at Chilton, near Harwell; even though the whole of the Atlas computer is used on a non-time-sharing basis it takes more than 4 hours to carry out the integrations required to produce a 24-hour forecast.

2.2. *The atmosphere as represented in the 10-level model*

The co-ordinate system used in the model is the following: horizontal co-ordinates (x, y) are taken on a stereographic map projection with the origin at the North Pole whilst pressure, p, is used as the vertical ordinate. A vertical resolution of 100 mb was chosen, the model atmosphere being bounded by the 1000-mb and the 100-mb levels; the contour fields of the 10 pressure levels taken together define the thermal structure of the model atmosphere at any given time. A horizontal grid length of approximately 50 km was chosen but it should be noted that, since variables are known only at alternate grid points, the effective horizontal resolution is about 100 km. Horizontal components of wind $\mathrm{d}x/\mathrm{d}t$, $\mathrm{d}y/\mathrm{d}t$, written u,v, are used to define the horizontal flow at each of the 10 pressure levels. Humidity mixing ratio, r, was chosen as the moisture variable, the particular values used being mean values of r appropriate to the seven layers of thickness 100 mb between 1000 mb and 300 mb, the atmosphere being assumed dry above 300 mb; this assumption was regarded as being valid for the real atmosphere for the latitudes of the British Isles for most occasions. The thickness, h', of a 100-mb slab between adjacent levels of the atmospheric column above a grid point is a measure of the mean temperature of that 100-mb slab and the thermodynamic equation is expressed in terms of layer thickness. The quantities h (or h'), u,v,r, constitute the dependent variables. The rate of vertical displacement of air is evaluated from $\mathrm{d}p/\mathrm{d}t$, which is written ω and is obtained when required via the continuity equation as indicated in the next section.

The present methods for treating condensation of water vapour and evaporation of rain and for incorporating surface friction, topography, lateral diffusion, sub-grid-scale convection, and heat and moisture transfers across the bottom boundary are dealt with in the later sections.

In all formulations the assumption has been made that the 1000-mb surface is completely in the fluid.

3. SYSTEM OF EQUATIONS

The form in which the equations are used is consistent with that originally proposed by Bushby and Timpson;[4] it does not correspond to a strict transformation from the surface of the sphere to the stereographic map projection. One consequence is that the balance equation appropriate to the system has a special form (Benwell and Bretherton,[5] see Section 5).

3.1. *Equations*

(i) *Equations of motion.* These are

$$u_t + m(uu_x + vu_y + gh_x) + \omega u_p - fv = g(\tau_X)_p + K(u_{xx} + u_{yy}), \quad \ldots (1)$$

$$v_t + m(uv_x + vv_y + gh_y) + \omega v_p + fu = g(\tau_Y)_p + K(v_{xx} + v_{yy}), \quad \ldots (2)$$

Further details about the incorporation of friction and lateral diffusion will be found in Section 6.

(ii) *Equation of continuity.* This is used in the form

$$m(u_x + v_y) + \omega_p = 0. \quad \ldots (3)$$

The value of ω at each level is obtained by integrating with respect to pressure, p, by using the trapezium rule. The boundary condition at 100 mb is taken as $\omega_{100} = 50\,(\omega_p)_{100}$ which is consistent with $\omega = \omega_p = 0$ at $p = 0$.

(iii) *Thermodynamic equation.* This is written as

$$h'_t + m(uh'_x + vh'_y) + \omega h'_p + \frac{\omega h'}{p}(1-\kappa) = \frac{\kappa b}{pg}Q + K(h'_{xx} + h'_{yy}), \quad \ldots (4)$$

where Q is the rate of non-adiabatic heating and includes

(*a*) condensation and evaporation,
(*b*) heating from the surface, and
(*c*) heating due to sub-grid-scale convection.

(iv) *The 1000-mb height tendency equation.* This equation is derived from the surface boundary condition $w \equiv \mathrm{d}z/\mathrm{d}t = \mathbf{V}.\nabla H$ at 1000 mb, and takes the form

$$h_t + \omega h_p + mu(h_x - H_x) + mv(h_y - H_y) = K(h_{xx} + h_{yy}). \quad \ldots (5)$$

(v) *The water balance equation.* This is used as

$$r_t + m(ur_x + vr_y) + \omega r_p = W + K(r_{xx} + r_{yy}), \quad \ldots (6)$$

where W is the rate of change of humidity mixing ratio due to

(*a*) gain or loss due to condensation and evaporation,
(*b*) transfer from the surface, and
(*c*) transfer due to sub-grid-scale convection.

These equations are solved numerically by the finite-difference scheme described in Section 4.

3.2. *Lateral boundary control*

Up to the present time no attempt has been made to introduce real boundary changes at the lateral boundaries and the following procedure is applied. The time derivatives of the dependent variables on the lateral boundaries are assumed to be zero throughout the forecast period; in addition, the gradient, normal to the boundary, of the velocity component parallel to the boundary is assumed zero. This procedure would normally set up gravity waves with fast-growing amplitudes, but these spurious gravity waves are controlled by the use of an enhanced diffusion coefficient at all grid points within 300 km of the lateral boundaries, so that the waves are effectively removed before they can invade the inner computational area and cause computational instability.

4. FINITE-DIFFERENCE SCHEME

4.1. *The scheme*

The scheme used is similar to that described by Eliassen[6] with modifications as suggested by Phillips.[7] An essential feature of this scheme is that it is staggered in both time and space, as shown in Figure 1. The horizontal grid consists of 95×63 points approximately 50 km apart and there are 10 pressure levels in the vertical. Values of h, u and v are kept at each level whereas r and h' refer to the layers between adjacent levels.

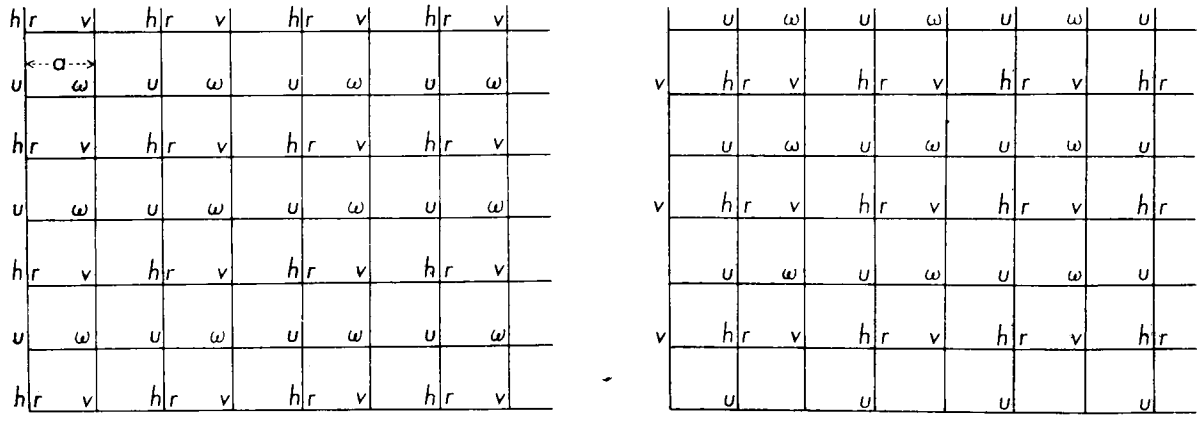

(*a*) Initially and after each double time-step
$r, h = 48 \times 32 = 1536$ $u = 48 \times 31 = 1488$
$v = 47 \times 32 = 1504$ $\omega = 47 \times 31 = 1457$
a = horizontal grid length

(*b*) At intermediate times
$r, h = 47 \times 31 = 1457$ $u = 47 \times 32 = 1504$
$v = 48 \times 31 = 1488$ $\omega = 46 \times 30 = 1380$

FIGURE 1. Horizontal array of data

There appears to be little virtue in introducing elaborate difference schemes in order to conserve momentum, mass or energy when the integrations are made for only relatively short periods of one or two days. Simple centred differences are used for the space derivatives except at the boundaries when one-sided differences are normally used. The only exception to this is in the evaluation of h'_p at 150 mb in equation (4). A one-sided difference is a very bad approximation of this term since the thickness of a 100-mb layer is increasing rapidly in this region, the thickness of the 100-mb layer above 100 mb being infinite. It was therefore decided to use a value of h'_p at 150 mb based on the International Civil Aviation

Organization (ICAO) Standard Atmosphere, and to correct for temperature departure from the standard by taking

$$h'_p = (h'_p)_{\text{ICAO}} \frac{h'}{h'_{\text{ICAO}}}.$$

When a variable or its derivative is required at a grid point, or a level, at a time for which it is not stored and is therefore unavailable, a simple average is taken of the values at the nearest grid points or adjacent levels for which the quantity is available. The examples of the algorithms set out in Appendix I show how these mean values enter into the computations.

Phillips[7] indicated that if a simple centred formula is used for the time derivatives then the nature of the equations is such that two distinct computational modes are set up, one for odd and the other for even time-steps, and this can lead to computational instability. The following system of integrating with respect to time has been adopted for all variables. This consists of an integration cycle of a forward time-step δt followed by a leap-frogging centred time-step of $2\delta t$; thus

$$u(t+\delta t) = u(t) + \overset{ND}{u_t}(t)\delta t \qquad \ldots (7)$$

$$u(t+2\delta t) = u(t) + 2\overset{ND}{u_t}(t+\delta t)\delta t + 2\overset{D}{u_t}(t)\delta t, \qquad \ldots (8)$$

where $\overset{ND}{u_t}(t)$ is the rate of change of u at time t, ignoring the effects of diffusion and $\overset{D}{u_t}(t)$ is the rate of change of u due entirely to horizontal diffusion. The reason for splitting the rate of change of the dependent variables into two parts is that diffusion equations are essentially stable with forward time-steps, whereas advective equations are essentially stable with centred time-steps. Equations (7) and (8) used in conjunction with Eliassen's scheme, are computationally stable for the linearized equations provided δt is sufficiently small; but it must be emphasized that such a system of integrating with respect to time is unstable unless some form of spatial smoothing similar to that implicit in Eliassen's scheme is incorporated in it, as it is equivalent to a forward time-step of $2\delta t$ with the second-order terms included for the advective rate of change.

There is another aspect of the method of solution which needs to be mentioned here. Starting with dependent variables h' and r at time t, new values are computed using the integration cycle above in conjunction with algorithms for equations (4) and (6), but assuming $Q = 0$ and $W = 0$. The effects of (*a*) condensation and evaporation, (*b*) transfers from the surface, and (*c*) changes due to sub-grid-scale convection are then introduced in that order and details of these procedures are given in Sections 7 to 9.

4.2. *Stability criterion*

The stability condition relating to fast-moving gravity waves in this scheme is given, in the absence of horizontal diffusion, by

$$\delta t \leqslant \delta x\{2(c^2 + V^2)\}^{-\frac{1}{2}},$$

where c is the speed of the gravity waves. A derivation of the time-step criterion appears in Appendix II, including the modification to allow for the inclusion of lateral diffusion. In practice most forecasts have been produced using a value of δt of 90 seconds; for most situations such a time step will suffice if the computation area does not extend further south than about 31 degrees north and if the value of the lateral diffusion coefficient does not

exceed 10^6 m^2/s. A check would, however, be necessary on occasions when the atmosphere at the most southerly part of the computation area is extremely warm or if a strong jet stream had penetrated to these southerly latitudes.

5. INITIALIZATION

5.1. *Introduction*

Specification of initial distributions of horizontal wind, pressure-surface contour heights and humidity mixing ratio are required before the equations of motion ((1), (2)) can be solved. However, a set of initial conditions which is apparently suitable for use in the prediction of large-scale flow may, in practice, contain slight inconsistencies which excite other (usually small-amplitude) physical processes to an exaggerated and unrealistic extent. The equations are particularly sensitive to small-scale roughnesses in the horizontal, to static instability in the vertical and to an incorrect balance between wind and pressure gradient, and it is important to ensure that the initial data are free from these defects before starting a forecast.

The preparation of initial data for the 10-level model involves four main stages:

(i) Analysis of pressure-surface contours and relative humidities at standard levels.
(ii) Interpolation to levels used in the model.
(iii) Smoothing and convective adjustment.
(iv) Computation of non-divergent and irrotational wind components and vertical velocity from the balance equation, the ω-equation and the continuity equation.

Ideally all four stages would be included in a general objective analysis scheme; however, the present procedure is to treat them as separate steps in the initialization programme.

5.2. *Analysis and interpolation*

The majority of forecasts so far performed with the 10-level model have used subjectively analysed initial data. However, a number of 24-hour forecasts starting from objective analyses of contours both of the isobaric surfaces and of the humidities have been obtained, and the results are highly encouraging.

In the subjective analyses, contours are drawn at the following standard levels: 1000, 850, 700, 500, 400, 300, 200 and 100 mb; while humidity is analysed at only five standard levels, i.e. 1000 mb to 400 mb. For the humidity analyses it is useful to take into account surface observations of cloud and weather, satellite cloud photographs and frontal analyses, and this is made easier by analysing relative humidity $X = r/r_s$ (instead of the mixing ratio r), the mixing ratio being computed at a later stage.

The analysed variables are interpolated to give values of the contour height and relative humidity at the non-standard levels used in the model. The interpolation formulae are as follows:

$$h_{900} = 0{\cdot}3714h_{1000} + 0{\cdot}6286h_{850} + 30{\cdot}65$$

$$h_{800} = 0{\cdot}7051h_{850} + 0{\cdot}2949h_{700} + 34{\cdot}615$$

$$h_{600} = 0{\cdot}566h_{700} + 0{\cdot}434h_{500} + 83{\cdot}0$$

$$X_{950} = \tfrac{2}{3}X_{1000} + \tfrac{1}{3}X_{850} \qquad X_{550} = \tfrac{1}{4}X_{700} + \tfrac{3}{4}X_{500}$$

$$X_{750} = \tfrac{1}{3}X_{850} + \tfrac{2}{3}X_{700} \qquad X_{450} = \tfrac{1}{2}X_{500} + \tfrac{1}{2}X_{400}$$

$$X_{650} = \tfrac{1}{4}X_{700} + \tfrac{3}{4}X_{500} \qquad X_{350} = X_{400}.$$

The contour height interpolation assumes an environment curve lying along the saturated adiabatic.

The objective analysis procedure analyses the variables directly at the levels required by the 10-level model, the above interpolation formulae being used implicitly by the scheme.

5.3. *Smoothing and convective adjustment*

(i) *Vertical smoothing.* The independent analysis of each pressure surface sometimes leads to inconsistencies between one level and another, and on some occasions these are so severe that the initial conditions are statically unstable at a number of grid points—an example of this is shown in Figure 2. If this situation is not corrected a form of spurious 'grid-scale convection' often arises during the forecast, leading to unrealistic vertical velocity patterns similar to those illustrated in Figure 3.

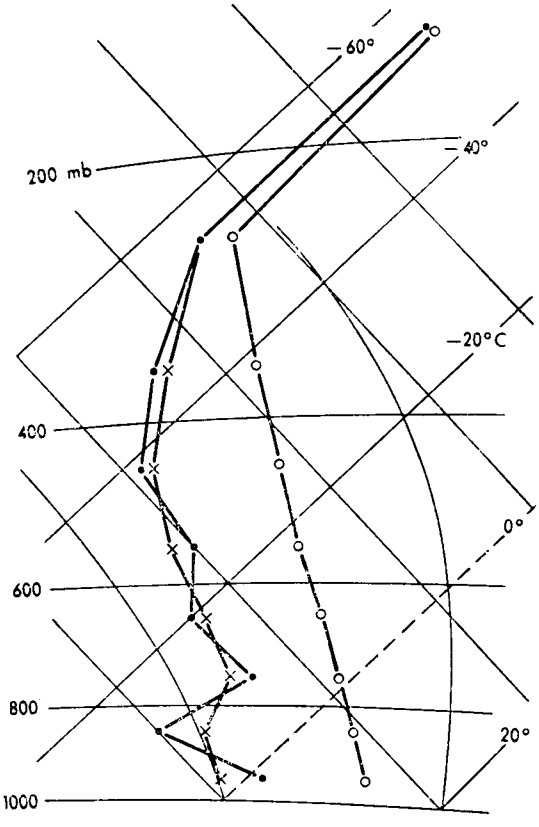

FIGURE 2. Typical soundings before and after vertical smoothing compared with equivalent sounding for the ICAO Standard Atmosphere

· ——— · Before vertical smoothing
× ——— × After vertical smoothing
o ——— o ICAO Standard Atmosphere equivalents

In the data preparation programmes for the 10-level model a vertical smoothing operator is applied which adjusts the vertical structure towards that of the standard static (ICAO) atmosphere (Benwell and Timpson[8]).

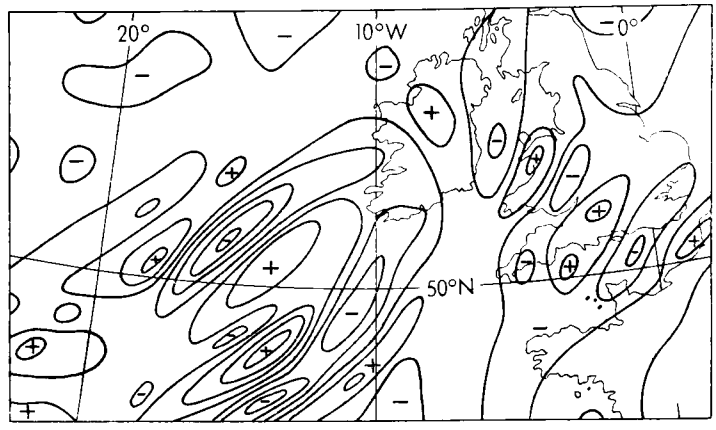

(*a*) Using initial data unsmoothed vertically. Isopleths at intervals of 200 mb/h.

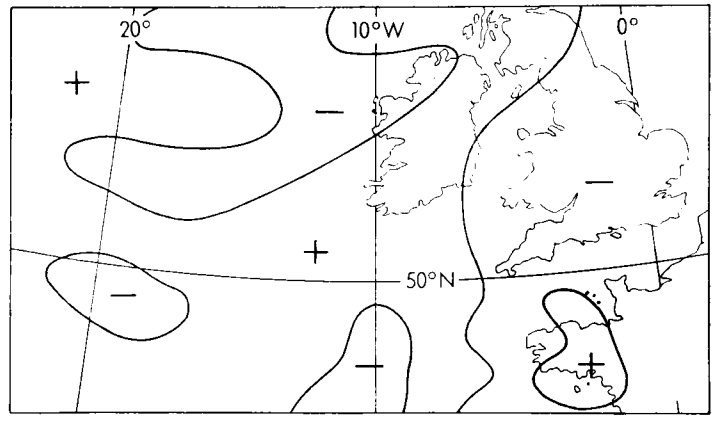

(*b*) Using initial data smoothed vertically. No motion > 25 mb/h.

FIGURE 3. 18-hour forecast of vertical velocity fields at 600 mb for 06 GMT on 26 December 1960

— Ascent + Descent

If the thickness of the layer in the ICAO Standard Atmosphere between pressure levels k and $k+1$ is written $(h'_{\mathrm{ICAO}})_{k+\frac{1}{2}}$, the distribution of

$$\Delta h'_{k+\frac{1}{2}} \equiv (h'_{\mathrm{ICAO}})_{k+\frac{1}{2}} - h'_{k+\frac{1}{2}}$$

is smoothed by applying the operator

$$(\Delta h'_{k+\frac{1}{2}})^* = \tfrac{1}{4}(\Delta h'_{k+\frac{3}{2}} + \Delta h'_{k-\frac{1}{2}}) + \tfrac{1}{2}\Delta h'_{k+\frac{1}{2}}, \qquad \ldots (9)$$

where the asterisk denotes the smoothed value. The operator (9) is applied in the six layers centred at 350 mb, 450 mb, . . . , 850 mb (i.e. for $k = 3, 4, \ldots, 8$), but a 'one-sided' smoothing operator is applied at 250 mb and 950 mb, as follows:

$$(\Delta h'_{250})^* = \tfrac{1}{4}\Delta h'_{350} + \tfrac{3}{4}\Delta h'_{250} \qquad (\Delta h'_{950})^* = \tfrac{1}{4}\Delta h'_{850} + \tfrac{3}{4}\Delta h'_{950}.$$

No smoothing is applied to the stratospheric layer centred at 150 mb since it tends to produce excessive changes in the neighbourhood of the tropopause.

The effect of the smoothing operator is illustrated in Figure 2. It is worth mentioning that the height changes brought about by the vertical smoothing amount to only a few metres—for example, in the case illustrated in Figure 2, the 900-mb height is decreased by 11 metres and the height of the 800-mb level is increased by 5 metres, although the corresponding changes in the static stability are substantial. The considerable improvement in the resulting forecast is clearly illustrated in Figure 3.

It is expected that the need for vertical smoothing will be much reduced, if not eliminated altogether, when objective analyses of each level are used. However, what is really required is a three-dimensional analysis scheme, with particular attention being paid to the correct representation of lapse rates.

(ii) *Convective adjustment.* Since, even after vertical smoothing, the distributions of thickness and humidity may imply instability with respect to the saturated adiabatic lapse rate, a convective adjustment procedure is also applied to the initial data. The procedure is similar to that adopted in the main forecast programme (described in Section 9); it consists of calculating the lapse rate $\gamma = -\partial T/\partial z$ and comparing it with a neutral lapse rate γ_c which is intermediate between the dry and the saturated adiabatic lapse rates and depends on the relative humidity according to the formula of equation (53). If $\gamma \leqslant \gamma_c$ no action is taken, but if $\gamma > \gamma_c$ then the thicknesses are adjusted so that

(*a*) $\gamma = \gamma_c$ and

(*b*) the total thickness $\sum_{k=1}^{9} h'_{k+\frac{1}{2}}$ remains unchanged. The relative humidity is left unaltered during the process.

The main advantage of convectively adjusting the data before starting a forecast is that this procedure eliminates a sudden readjustment of lapse rate as well as the production of spurious convective rainfall which would otherwise be produced during the first few time-steps.

(iii) *Horizontal smoothing.* The horizontal smoothing procedure has been described by Benwell and Timpson.[8] The smoothing operator (Wallington[9])

$$h_i^* = \frac{s}{2}(h_{i-1}+h_{i+1})+(1-s)h_i$$

is applied first along lines of grid points parallel to the x-axis and then along lines parallel to the y-axis; h_i^* and h_i are the smoothed and unsmoothed heights at grid point i while h_{i+1} and h_{i-1} are the unsmoothed heights at the adjacent grid points along the direction in which the smoothing operation is carried out. Two complete double sweeps are made, the first with $s = \frac{1}{2}$ and the second with $s = -\frac{2}{3}$. The technique damps out small-scale roughnesses (in particular waves of double grid-length, 4*a*) but leaves long wavelengths relatively unchanged. Relative humidities are horizontally smoothed in a similar way.

5.4 *Derivation of the balance equation and the ω-equation*

Thompson[10] has shown that for small-amplitude perturbations the necessary and sufficient condition for a rotating atmosphere in hydrostatic balance to be unable to support the propagation of gravity waves is that a relationship between the wind and pressure exists to make the total rate of change of the divergence of the horizontal wind

zero. In general this condition does not hold and the primitive equations are capable of predicting the motion of gravity waves. However, when analysing the initial conditions it is not easy to distinguish between the actual fine adjustments between wind and pressure distributions which allow the propagation of small-amplitude gravity waves as observed in the atmosphere, and slightly different wind and pressure distributions which lead to the production of waves with unrealistically large amplitudes. For this reason it is considered prudent to eliminate gravity waves completely during the initial stages of the forecasts. This is achieved by imposing the two initial conditions:

$$\frac{\mathrm{d}D}{\mathrm{d}t} \equiv \left\{\frac{\partial}{\partial t}+m\left[u\frac{\partial}{\partial x}+v\frac{\partial}{\partial y}\right]+\omega\frac{\partial}{\partial p}\right\}D = 0 \qquad \ldots (10)$$

and

$$\frac{\partial}{\partial t}\left\{\frac{\mathrm{d}D}{\mathrm{d}t}\right\} = 0, \qquad \ldots (11)$$

(where $D = u_x+v_y$ is the divergence) which ensure the maintenance of Thompson's condition throughout the first time-step.

Conditions (10) and (11) may be converted into purely diagnostic relationships between u, v, ω and h by using the equations of motion and thermodynamics to eliminate explicit reference to time derivatives. Considering equation (10) first, the equations of motion ((1), (2)) are used to eliminate $\partial u/\partial t$ and $\partial v/\partial t$ and obtain, after a minor approximation, the balance equation (ignoring friction and diffusion)

$$m(u_x{}^2+2v_xu_y+v_y{}^2)-f\zeta+mg\nabla^2h+\mathbf{k}\times\mathbf{V}.\nabla f+g\nabla m.\nabla h = 0. \qquad \ldots (12)$$

This expresses a balance between the geopotential field and the wind field taking into account the earth's rotation, the centrifugal force along curved trajectories, and ageostrophic deflexion due to accelerations in regions of confluence and diffluence.

The second initial condition (11) now becomes

$$\frac{\partial}{\partial t}[m(u_x{}^2+2v_xu_y+v_y{}^2)-f\zeta+mg\nabla^2h+\mathbf{k}\times\mathbf{V}.\nabla f+g\nabla m.\nabla h] = 0.$$

For consistency this equation should be used as it stands, but the present practice is to include only the most important terms to give the approximate condition

$$\frac{\partial}{\partial t}[-f\zeta+mg\nabla^2h] = 0. \qquad \ldots (13)$$

This may be combined with the vorticity equation and thermodynamic equation to eliminate $\partial\zeta/\partial t$ and $\partial h/\partial t$.

The vorticity equation for the 10-level model is (neglecting friction and diffusion)

$$\frac{\partial}{\partial t}(m\zeta)+m\mathbf{V}.\nabla(m\zeta+f)-(m\zeta+f)\frac{\partial\omega}{\partial p}+\omega\frac{\partial}{\partial p}(m\zeta)+$$
$$+m\mathbf{k}.\nabla\omega\times\frac{\partial\mathbf{V}}{\partial p}+m\mathbf{k}.\nabla m\times\nabla(\tfrac{1}{2}\mathbf{V}^2+gh) = 0. \qquad \ldots (14)$$

The last two terms can, however, be neglected since one involves $\nabla\omega$, which is small, and the other contains ∇m, which is also small and on the whole is parallel to $\nabla(\frac{1}{2}\mathbf{V}^2+gh)$.

Neglecting non-adiabatic effects the thermodynamic equation may be written in differential form

$$\frac{\partial}{\partial t}\frac{\partial h}{\partial p}+m\mathbf{V}.\nabla\frac{\partial h}{\partial p}+\frac{\sigma}{g}\omega=0, \qquad \ldots (15)$$

where

$$\sigma=-\frac{1}{\rho}\frac{\partial(\log\Theta)}{\partial p}$$

is a measure of the static stability.

Equations (13), (14) and (15) are now combined to eliminate $\partial\zeta/\partial t$ and $\partial h/\partial t$, and with a slight approximation the following equation for ω is obtained

$$m^2\nabla^2(\sigma\omega)+f(m\zeta+f)\frac{\partial^2\omega}{\partial p^2}+gm^2\nabla^2\left[m\mathbf{V}.\nabla\frac{\partial h}{\partial p}\right]-fm\frac{\partial}{\partial p}[\mathbf{V}.\nabla(m\zeta+f)]=0. \qquad \ldots (16)$$

Since the static stability is, to a large extent, a function of p only, horizontal variations are neglected and a distribution for σ is computed from data for the ICAO Standard Atmosphere (see Table I). This greatly simplifies the computational problems.

TABLE I. *The static stability, σ, as a function of pressure, calculated from the ICAO Standard Atmosphere*

Pressure *mb*	Static stability, σ $m^2/mb^2\,s^2$
100	$135{\cdot}0360\times10^{-2}$
200	$30{\cdot}9767\times10^{-2}$
300	$7{\cdot}2873\times10^{-2}$
400	$4{\cdot}1618\times10^{-2}$
500	$2{\cdot}5973\times10^{-2}$
600	$2{\cdot}1545\times10^{-2}$
700	$1{\cdot}4800\times10^{-2}$
800	$1{\cdot}1815\times10^{-2}$
900	$0{\cdot}9320\times10^{-2}$
1000	$0{\cdot}7485\times10^{-2}$

Equations (12) and (16) together with the continuity equation

$$m\left[\frac{\partial u}{\partial x}+\frac{\partial v}{\partial y}\right]+\frac{\partial\omega}{\partial p}=0 \qquad \ldots (17)$$

form a set of three equations in the three unknowns u, v and ω (the contour height h is regarded as being given). Although in principle they may be solved simultaneously, the amount of computation involved is formidable. Instead of this the wind $\mathbf{V}$ may be split into two components (a non-divergent part, $\mathbf{V}'$, and an irrotational part, $\mathbf{V}''$)

$$\mathbf{V}=\mathbf{k}\times\nabla\psi+\nabla\chi=\mathbf{V}'+\mathbf{V}''. \qquad \ldots (18)$$

Because the flow is approximately geostrophic $|\nabla\psi|\gg|\nabla\chi|$, and so, if equation (18) is used to substitute for u_x, u_y, v_x, v_y, ζ and $\mathbf{V}$ in the balance equation (12), and if any term involving gradients of χ is neglected, the following equation is obtained

$$2m(\psi^2{}_{xy}-\psi_{xx}\psi_{yy})-f\nabla^2\psi+mg\nabla^2h-\nabla\psi.\nabla f+g\nabla m.\nabla h=0. \qquad \ldots (19)$$

This may be solved as a boundary value problem if it is elliptic, i.e. provided that

$$m^2g\nabla^2h+\frac{f^2}{2}-m\nabla\psi.\nabla f+mg\nabla m.\nabla h > 0. \quad \ldots (20)$$

Since equation (19) may be written

$$\nabla^2\psi = -\frac{f}{m}\pm\left[\frac{f^2}{m^2}+4\psi^2_{xy}+(\psi_{xx}-\psi_{yy})^2+2g\nabla^2h-\frac{2}{m}\nabla\psi.\nabla f+\frac{2g}{m}\nabla m.\nabla h\right]^{\frac{1}{2}}, \quad \ldots (21)$$

condition (20) is sufficient to ensure a real solution to equation (21). The positive root (which implies non-negative absolute vorticity) is the meteorological mode in the northern hemisphere. In practice, however, condition (20) is replaced by the approximate condition

$$m^2g\nabla^2h+\frac{f^2}{2}-\frac{m^2g}{f}\nabla h.\nabla f+mg\nabla m.\nabla h-\epsilon > 0, \quad \ldots (22)$$

where the geostrophic term $(mg/f)\nabla h$ takes the place of $\nabla\psi$ and the positive parameter ϵ compensates for any discrepancy introduced by the approximation. This condition is tested at every point and the height field altered if necessary to ensure ellipticity everywhere. The parameter ϵ is taken to be proportional to the Coriolis parameter ($\epsilon/f \approx 2\times10^{-6}$/s) so that 'over-ellipticization' is reduced in low latitudes (otherwise excessive height changes might be required there). The ellipticization is started at 1000 mb and any changes in the contour field are added to the level above before that field itself is ellipticized and this helps to preserve the temperature structure. When the stream function ψ has been found from equation (19), equation (18) is substituted into the ω-equation, terms involving χ again being neglected, to give

$$m^2\sigma\nabla^2\omega+f(m\zeta+f)\frac{\partial^2\omega}{\partial p^2} = mf\frac{\partial}{\partial p}\left[\mathbf{V}'.\nabla(m\zeta+f)\right]-m^2g\nabla^2\left[m\mathbf{V}'.\nabla\frac{\partial h}{\partial p}\right]. \quad \ldots (23)$$

This is elliptic if

$$\frac{f(m\zeta+f)}{\sigma} > 0.$$

The vertical velocity ω given by equation (23) is now substituted into the continuity equation to give a Poisson equation for the velocity potential χ

$$m\nabla^2\chi+\frac{\partial\omega}{\partial p} = 0. \quad \ldots (24)$$

When a value of χ has been obtained from equation (24) it would be possible to proceed iteratively to a solution by using this value to estimate the terms in the balance equation which were previously neglected and then computing a new estimate for the stream function ψ. However, an approximate solution based on only one iteration is considered sufficiently accurate for initialization purposes.

5.5 *Finite-difference solution of the initialization equations*

(i) *The balance equation.* Great care must be taken to ensure consistency with the model's prognostic equations and to achieve this the balance equation is rederived

directly from the finite-difference equations of motion. The algebraic manipulation involved is tedious and will not be reproduced here but the technique is simple and consists of subtracting the appropriate finite-difference equations of motion at neighbouring points to obtain a finite-difference expression for

$$\frac{\partial}{\partial t}\left(\frac{\partial u}{\partial x}+\frac{\partial v}{\partial y}\right)=0.$$

A stream function ψ (defined at the 'h' points of the grid) is then introduced for the wind field to give the equation

$$A\psi(i,j)^2+B\psi(i,j)+C=0, \qquad \ldots (25)$$

where

$$A=-\frac{1}{16a^4}[m(i,j+1)+m(i,j-1)+m(i+1,j)+m(i-1,j)];$$

$$\begin{aligned}B=\frac{1}{32a^4}&[m(i+1,j)\{\psi(i+2,j+2)+\psi(i,j+2)+\psi(i+2,j-2)+\psi(i,j-2)\}+m(i-1,j)\times\\&\times\{\psi(i,j+2)+\psi(i-2,j+2)+\psi(i,j-2)+\psi(i-2,j-2)\}+m(i,j+1)\{\psi(i+2,j)+\\&+\psi(i+2,j+2)+\psi(i-2,j)+\psi(i-2,j+2)\}+m(i,j-1)\{\psi(i+2,j)+\psi(i+2,j-2)+\\&+\psi(i-2,j)+\psi(i-2,j-2)\}]+\frac{1}{4a^2}[f(i-1,j)+f(i+1,j)+f(i,j+1)+f(i,j-1)];\end{aligned}$$

$$\begin{aligned}C=\frac{1}{128a^4}&[m(i+1,j)\{\psi(i+2,j+2)-\psi(i+2,j-2)\}^2+m(i-1,j)\{\psi(i-2,j+2)-\\&-\psi(i-2,j-2)\}^2+m(i,j+1)\{\psi(i+2,j+2)-\psi(i-2,j+2)\}^2+m(i,j-1)\times\\&\times\{\psi(i+2,j-2)-\psi(i-2,j-2)\}^2-\{m(i+1,j)+m(i-1,j)\}\{\psi(i,j+2)-\psi(i,j-2)\}^2-\\&-\{m(i,j+1)+m(i,j-1)\}\{\psi(i+2,j)-\psi(i-2,j)\}^2+4m(i+1,j)\psi(i+2,j)\times\\&\times\{2\psi(i+2,j)-\psi(i+2,j+2)-\psi(i+2,j-2)-\psi(i,j+2)-\psi(i,j-2)\}+\\&+4m(i-1,j)\psi(i-2,j)\{2\psi(i-2,j)-\psi(i-2,j+2)-\psi(i-2,j-2)-\\&-\psi(i,j+2)-\psi(i,j-2)\}+4m(i,j+1)\psi(i,j+2)\{2\psi(i,j+2)-\psi(i+2,j+2)-\\&-\psi(i-2,j+2)-\psi(i+2,j)-\psi(i-2,j)\}+4m(i,j-1)\psi(i,j-2)\{2\psi(i,j-2)-\\&-\psi(i+2,j-2)-\psi(i-2,j-2)-\psi(i+2,j)-\psi(i-2,j)\}]-\\&-\frac{1}{4a^2}[f(i+1,j)\psi(i+2,j)+f(i-1,j)\psi(i-2,j)+f(i,j+1)\psi(i,j+2)+f(i,j-1)\psi(i,j-2)]+\\&+\frac{g}{4a^2}[m(i+1,j)h(i+2,j)+m(i-1,j)h(i-2,j)+m(i,j+1)h,(i,j+2)+m(i,j-1)h(i,j-2)]-\\&-\frac{g}{4a^2}\{m(i+1,j)+m(i-1,j)+m(i,j+1)+m(i,j-1)\}h(i,j);\end{aligned}$$

and where terms in ω are neglected.

Choosing the root of the quadratic equation (25) appropriate for positive absolute vorticity gives

$$\nabla^2\psi = \frac{1}{4a^2}\left[\psi(i+2,j)+\psi(i,j+2)+\psi(i,j-2)+\psi(i-2,j)+\frac{2}{A}\{B-(B^2-4AC)^{\frac{1}{2}}\}\right] \equiv \mathrm{F}(\psi) \quad \ldots (26)$$

where $$\nabla^2\psi \equiv \frac{1}{4a^2}\{\psi(i+2,j)+\psi(i,j+2)+\psi(i,j-2)+\psi(i-2,j)-4\psi(i,j)\},$$

and equation (26) is a finite-difference representation of equation (21). Equation (26) is now solved using the iterative procedure

$$\nabla^2\psi^{(n+1)} = \alpha\nabla^2\psi^{(n)}+(1-\alpha)\mathrm{F}(\psi^{(n)}). \quad \ldots (27)$$

Since the technique has a tendency to oscillate with successive iterations about the solution, the parameter α is taken to be positive (namely 0·4), corresponding to a process of under-relaxation.

If the iterations show signs of diverging, α is increased to 0·6. Alternating-direction implicit methods are used to solve the Poisson equation at each iteration.

A first guess is obtained by solving the linear balance equation

$$-f\nabla^2\psi+mg\nabla^2h-\nabla\psi.\nabla f+g\nabla m.\nabla h = 0, \quad \ldots (28)$$

while around the boundary $\psi = (mgh/f)+\delta$ is used, where δ is an adjustment increment added at each boundary grid-point to ensure that the line integral of the inflow vanishes.

Occasionally difficulties arise because the radicand in the expression for F (ψ) becomes negative during the iterative procedure. This sometimes happens during the first few iterations if the solution of equation (28) does not provide a sufficiently good guess, or alternatively it can occur near the edges of the region of integration where the assumption of geostrophic conditions around the boundary is inconsistent with balanced winds in the interior. In addition, negative numbers under the square root in equation (26) may arise later in the iterative process if the approximate ellipticity condition (22) is insufficient to ensure that the full finite-difference balance equation is elliptic. In such circumstances the square-root term is set equal to zero at the grid points in question, though a better procedure might be to re-ellipticize using the current estimate for ψ and to adopt boundary conditions consistent with the gradient wind rather than with the geostrophic wind. The iterative procedure (27) usually converges in about 20 iterations, though in specific cases (e.g. when difficulties arise with the square-root term) it takes more.

(ii) *The ω-equation.* Since the presence of initial vertical velocities is found to have only a small effect on the forecast after two or three hours (see Section 5.6.) an elaborate finite-difference scheme to ensure consistency of the equation with the finite-difference forecast equations is unnecessary. Therefore a simple centred differencing scheme for the derivatives in equation (16) is adopted.

Writing

$$A_1 = \frac{f(m\zeta+f)}{m^2\sigma},$$

and

$$A_2 = \frac{f}{m\sigma}\frac{\partial}{\partial p}[\mathbf{V}'.\nabla(m\zeta+f)]-\frac{g}{\sigma}\nabla^2\left[m\mathbf{V}'.\nabla\frac{\partial h}{\partial p}\right],$$

the ω-equation becomes

$$\nabla^2\omega + A_1\frac{\partial^2\omega}{\partial p^2} = A_2.$$

This is solved with the iterative scheme

$$\omega^{(n+1)}(i-1,j-1,k) = \alpha\omega^{(n)}(i-1,j-1,k)+(1-\alpha)G,$$

where α is a constant and

$$G = \frac{100^2}{4+8a^2A_1}\left[\frac{4a^2A_1}{100^2}[\omega(i-1,j-1,k-1)+\omega(i-1,j-1,k+1)]-\right.$$
$$\left.-4a^2A_2+\omega(i+1,j-1,k)+\omega(i-3,j-1,k)+\omega(i-1,j+1,k)+\omega(i-1,j-3,k)\right].$$

An over-relaxation scheme with $\alpha = -\frac{1}{3}$ is found to converge rapidly.

The boundary conditions for the ω-equation are necessarily artificial; however, the conditions of zero ω on the lateral boundaries and at $p = 100$ mb are unlikely to have any adverse effect except in the immediate neighbourhood of the boundaries. At 1000 mb the boundary condition for the 10-level model is $w = m\mathbf{V}_{1000}.\nabla H$ and this leads to the tendency equation

$$\frac{\partial h_{1000}}{\partial t}+m\mathbf{V}_{1000}.\nabla h_{1000}+\omega\frac{\partial h_{1000}}{\partial p} = m\mathbf{V}_{1000}.\nabla H,$$

but in the absence of gravity waves $\partial h_{1000}/\partial t$ is small. Thus, with a slight approximation the following lower boundary condition for the ω-equation is obtained

$$-mh_{1000}\nabla.\mathbf{V}''_{1000}+\omega_{1000}\frac{\partial h_{1000}}{\partial p}-m\mathbf{V}'_{1000}.\nabla(H-h_{1000}) = m\mathbf{V}''_{1000}.\nabla H-m\nabla.(h_{1000}\mathbf{V}''_{1000}).$$

The two terms on the right-hand side (which involve advection by the irrotational part of the wind) are small and may be neglected; however, the first term on the left-hand side has an overall effect since the 1000-mb contour height and the divergence have a net positive correlation. Then

$$\omega_{1000} = \omega_{900}\frac{h_{1000}}{h_{1000}-h'_{950}}+\frac{100m\mathbf{V}'_{1000}.\nabla(H-h_{1000})}{h_{1000}-h'_{950}},$$

where use has been made of the continuity equation and vertical derivatives have been replaced by one-sided finite differences.

(iii) *The velocity potential equation.* The velocity potential χ is calculated only at 'ω' points of the 10-level model grid. An over-relaxation scheme to solve the Poisson equation (24) converges rapidly.

The total wind may now be found from

$$u(i,j-1) = \frac{1}{2a}[\psi(i,j-2)-\psi(i,j)+\chi(i+1,j-1)-\chi(i-1,j-1)],$$

$$v(i+1,j) = \frac{1}{2a}[\psi(i,j)-\psi(i+2,j)+\chi(i+1,j+1)-\chi(i+1,j-1)].$$

As a final check to ensure consistency with the 10-level model equations, the vertical velocity ω is recomputed from the total wind by integrating the continuity equation using the same numerical technique as that of the forecasting procedure (equation (3)).

5.6. *Discussion on the influence of balanced winds*

Early forecasts with the 10-level model were performed with initial non-divergent winds and with the vertical velocity identically zero everywhere (Bushby and Timpson[4]). The stream function was obtained from the linear balance equation

$$\nabla^2\psi = \frac{mg}{f}\nabla^2 h. \qquad \ldots (29)$$

However, the forecasts were found to possess an oscillation with a period of about $4\frac{1}{2}$ hours (Figure 4). This was identified by Benwell and Bretherton[5] as an external standing gravity wave having a half wavelength equal to the distance between the side boundaries

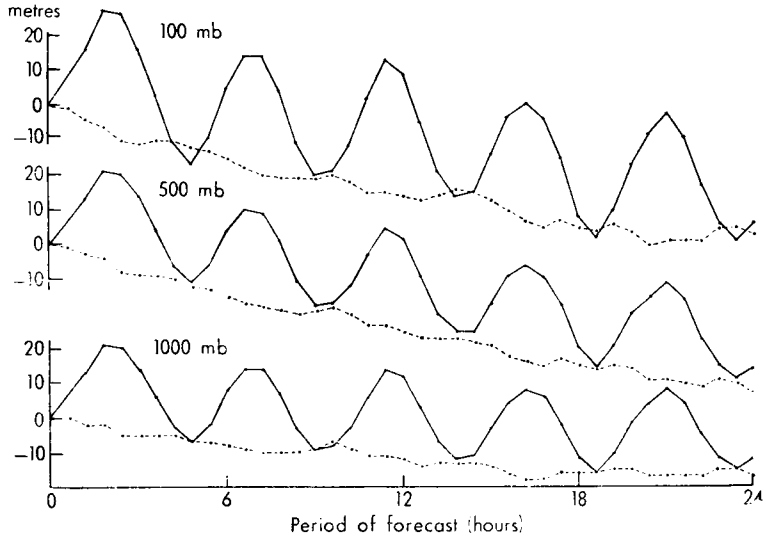

FIGURE 4. Variations in mean heights of the 1000, 500 and 100-mb isobaric surfaces over the computation area during the 24-hour forecast, with and without gravity wave oscillation

——— With gravity wave oscillation - - - Without gravity wave oscillation
Initial data 00 GMT on 1 December 1961.

and an amplitude increasing with height. They diagnosed the cause to be the neglect in equation (28) of the additional terms, $-\nabla\psi.\nabla f+g\nabla m.\nabla h$, which are locally small but which make a net overall contribution because the wind and contour lines tend to lie, on average, along lines of latitude, i.e. perpendicular to ∇f and ∇m. When the stream function is calculated from the full linear balance equation ((28)) the oscillation does not appear (Figure 4).

The effect of starting the forecast with non-zero vertical velocities (obtained from the ω-equation) is shown in Figure 5. After about $1\frac{1}{2}$ hours the distribution of the areal mean of the modulus of ω in the forecast having $\omega \equiv 0$ initially is very similar to that obtained

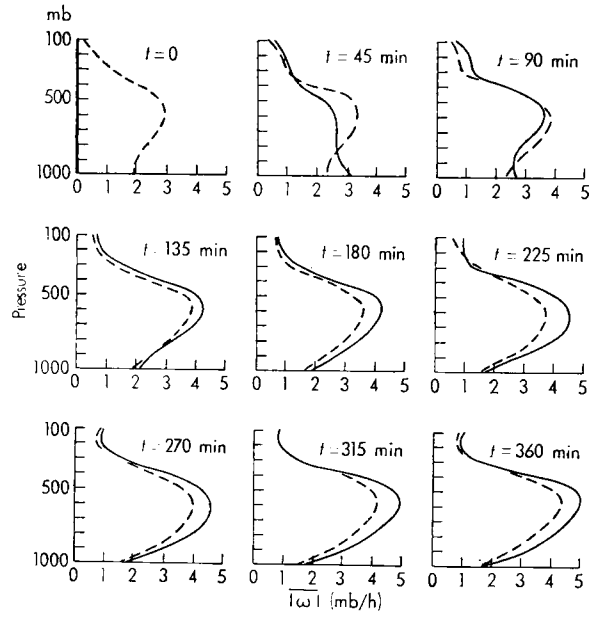

FIGURE 5. Profiles of the area mean of the modulus of vertical velocity, $|\overline{\omega}|$, at intervals of 45 minutes in the first 6 hours of a forecast, for different initial conditions

——— Behaviour using zero initial vertical motion

– – – Behaviour when initial vertical motions were obtained from the ω-equation

$\overline{|\omega|}$ was averaged over the computation area excluding part within 300 km of the lateral boundary.

by starting with vertical velocities given by the ω-equation, and subsequently the profiles remain substantially the same (although small differences are evident). This provides a measure of the initial dynamical adjustment period of the model.

The linear balance equation ((28)) gives a satisfactory stream function in general, although in certain synoptic situations some difficulties have arisen. An example is the forecast starting at 00 GMT on 15 September 1968. A depression situated in the Bay of Biscay moved slowly north-east with little change in pressure. In the 10-level model forecast the central pressure dropped sharply by 10 mb or so during the first hour (Figure 6)

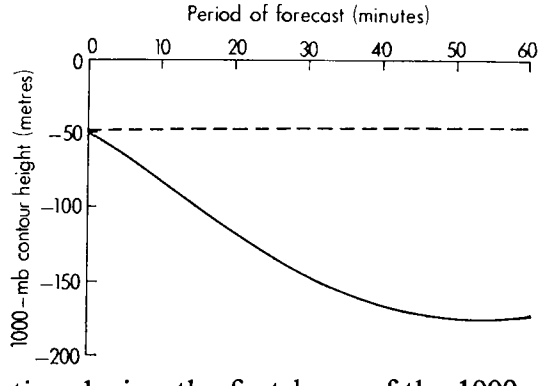

FIGURE 6. Forecast evolution during the first hour of the 1000-mb contour height at the centre of a depression in the Bay of Biscay using initial winds for 00 GMT on 15 September 1968 derived from the linear balance equation and from the non-linear balance equation

——— Linear balance equation – – – Non-linear balance equation

although the movement was fairly well predicted. In spite of this initial pressure drop, the final forecast proved to be quite good, although the central pressure was still too low. A forecast starting with winds obtained from the full non-linear balance equation ((19)) did not show this initial pressure drop and the forecast behaviour agreed closely with the actual (Figure 6). It was notable that away from the depression the two forecasts differed little from each other, showing that the non-linear terms are important only locally. This may be seen to be so by writing the balance equation ((12)) in the form

$$\frac{m}{2}(D^2+\mathrm{def}^2-\zeta^2)-f\zeta+mg\nabla^2 h+\mathbf{k}\times\mathbf{V}.\nabla f+g\nabla m.\nabla h=0$$

where $\mathrm{def}^2=(u_x-v_y)^2+(v_x+u_y)^2$ is the square of the total deformation. It is clear that the non-linear terms become important when either the deformation or the vorticity is large (greater than $2f$). Such magnitudes only arise in limited regions of the flow field; in the case quoted above, for example, the maximum vorticity was about $4f$ and vorticities greater than $2f$ occupied only about four or five grid points.

For some experiments a simple centred differencing scheme was used in the balance equation. However, when this was replaced by the more complicated (but more consistent) system given in Section 5.5.(i) the result was the removal of a spurious pressure surge during the first two hours of the forecast (see Figure 7).

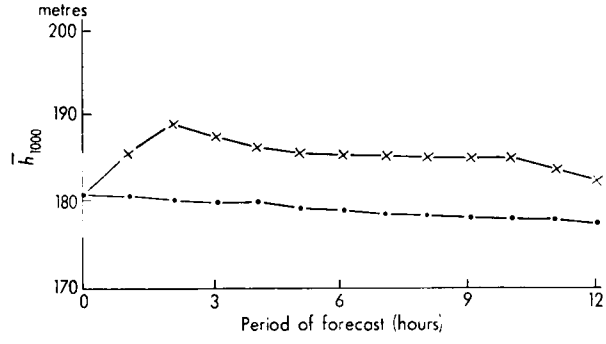

FIGURE 7. Variation of mean height of 1000-mb surface during the first 12 hours of forecast using initial winds derived from the full balance equation with simple centred differencing scheme and from a formulation of the full balance equation consistent with the finite-difference form of the equations of motion (Section 5.5.(i))

× ——— × Full balance equation with simple centred differencing scheme
• ——— • Formulation of the full balance equation described in Section 5.5.(i)
Initial data 00 GMT on 10 July 1968.

The effect of different balance conditions on the rainfall prediction is less well marked. On comparing forecasts with zero and non-zero initial vertical velocities it was found that early in the forecast period a prediction starting with a distribution of ω obtained from the ω-equation had slightly less rainfall than that produced from a forecast with $\omega \equiv 0$ initially. This was apparently due to over-compensation during the initial adjustment period of the unbalanced forecast (starting a forecast with $\omega \equiv 0$ is equivalent to giving the atmosphere an initial impulsive shock of sufficient magnitude to destroy any vertical motion which would otherwise be present). A similar result becomes evident from a

comparison of results from initial conditions obtained from the linear balance equation ((28)) and the non-linear balance equation ((19)). For the case already mentioned (15 September 1968) the excessive deepening during the first hours of the forecast computed from initial data obtained by using the linear balance equation led to high wind speeds and to the production of spurious orographic rain over north Spain. The initial balance conditions had little discernible effect on the 12-hour or 24-hour forecast rates of rainfall, a much more important factor being the accuracy of the initial humidity analysis.

The initialization procedures described in this chapter entail some alteration to the basic raw initial data. However, this is largely necessary to eliminate errors introduced by the subjective analysis and grid-point interpolation, and it is expected that the smoothing may be considerably reduced in severity when consistent objective analyses are used. Nevertheless, even with the present scheme real synoptic features do not become excessively smoothed out. This can be seen in the cross-section through a front illustrated in Figure 8, where the principal effect is to reduce the extreme conditional instability in the warm air, while the horizontal intensity of the front remains much as before.

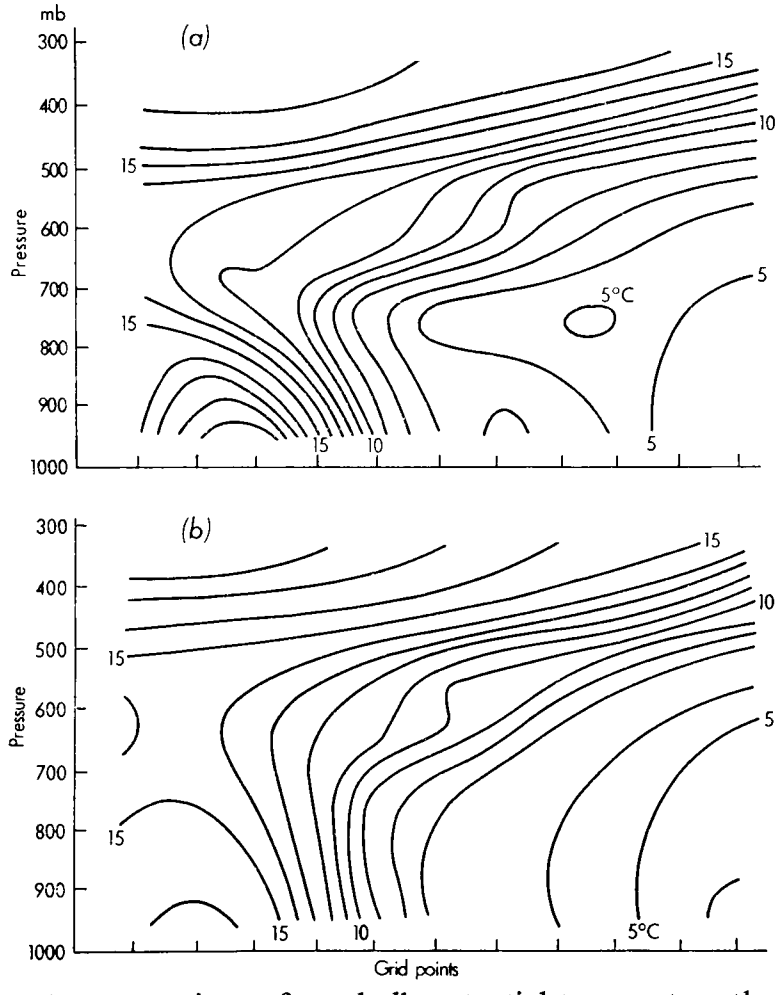

FIGURE 8. Vertical cross-sections of wet-bulb potential temperature through frontal zone
(*a*) From raw data (*b*) After initialization procedures
Initial data 00 GMT on 16 October 1967.

6. TOPOGRAPHY, FRICTION AND LATERAL DIFFUSION

These effects will be discussed in the order in which they were introduced into the model since this sequence had some effect on the particular formulations which have been adopted.

6.1. *Topography*

Topography was the first of these effects to be included. High ground causes a general ascent of the airflow over windward slopes and a general descent to leeward with, of course, some of the flow being diverted around mountain ranges. There will be other, smaller, effects as well due to the resistance to air motion caused by individual peaks and roughnesses; these effects are treated as a variation in the frictional resistance, and will be mentioned later in this section. The large-scale effects of topography are simulated in the model by modifying the lower boundary condition. This condition before the introduction of topographic effects was $w \equiv \mathrm{d}z/\mathrm{d}t = 0$ at 1000 mb but was changed to $w = \mathbf{V}.\mathrm{grad}\, H$ where H, the topography, is the height of the ground above MSL; this formulation is similar to that used by Krishnamurti.[11] The experiments in this case were therefore carried out to determine the most acceptable form for the H fields. In all the experiments H is taken as a value of the average height of the land above MSL over a grid square (of sides approximately 100 km). The procedure to obtain the basic H values was to determine the mean values subjectively from contour charts. For coastal regions of continents when the proportion of land to sea represented less than one-sixth of a grid square then the value of H was taken as zero; isolated islands falling within the grid square were ignored unless they occupied at least one-twelfth of the square. In the first experiments the H values used were for the grid-point arrays corresponding to the u and v arrays and the grid squares were overlapping as shown in Figure 9(*a*). It will be seen that the H_x, H_y terms at the forward and centred time-steps obtained by using this configuration of H values represent

(*a*) H at alternate points to those of initial 'h' field (*b*) H field identical with initial 'h' field

FIGURE 9. Configuration of topographic height used in experiments

the same scale of motion as that obtained from values at 100 km apart. When this configuration was used the computations became unstable in 12 hours. The alternative scheme, Figure 9(*b*), was to use H values at the h arrays, since in addition to requiring less storage space it was possible to use finite-difference approximations for H_x, H_y consistent with the approximations used elsewhere in the integrations. For the forward time-step H_x, H_y at point A are represented by

$$\frac{H_2+H_5-H_1-H_4}{2a} \text{ and } \frac{H_1+H_2-H_5-H_4}{2a} \text{ respectively.}$$

For the centred time-step H_x, H_y at point B are represented by

$$\frac{H_C+H_D-H_A-H_E}{2a} \text{ and } \frac{H_A+H_C-H_D-H_E}{2a},$$

i.e. $\dfrac{H_9+2H_6+H_3-H_1-2H_4-H_7}{8a}$ and $\dfrac{H_1+2H_2+H_3-H_9-2H_8-H_7}{8a}$ respectively.

It will be obvious that these finite-difference approximations involve some smoothing.

Despite the smoothing implicit in the finite-difference approximations, the use of these basic H fields in the early experiments led to some instability in the integrations, so it was considered that the removal, by smoothing, of the Fourier components corresponding to waves of only a few grid lengths would reduce the computational instability. Two versions of smoothing were used corresponding to the 9-point operator

$$\frac{1}{16}\begin{vmatrix} 1 & 2 & 1 \\ 2 & 4 & 2 \\ 1 & 2 & 1 \end{vmatrix}$$

and the 25-point operator

$$\frac{1}{144}\begin{vmatrix} 1 & 3 & 4 & 3 & 1 \\ 3 & 9 & 12 & 9 & 3 \\ 4 & 12 & 16 & 12 & 4 \\ 3 & 9 & 12 & 9 & 3 \\ 1 & 3 & 4 & 3 & 1 \end{vmatrix}.$$

The first operator corresponds to the application of a 3-point smoothing operator used by Shuman[12] (and Wallington[9]) (see page 9), applied in the x and y directions with $s = \frac{1}{2}$ and the second operator involves the further application of a 3-point operator in both the x and y directions with $s = \frac{2}{3}$. The first operator removes the roughnesses of double grid-length, $4a$, whilst the second removes, in addition, roughnesses of three grid-lengths, $6a$.

As mentioned earlier, when the basic values of H were used the integrations became unstable, and though the use of moderately smoothed H fields resulted in some improvement and gave realistic patterns the magnitudes of the vertical velocity, the lee troughs and other patterns increased gradually as the forecast proceeded and became unacceptable meteorologically by the 18-hour stage of the forecast. (It should, however, be borne in mind that at this point in the forecast formulation, lateral diffusion had not been incorporated.) From these experiments it appeared necessary to use the drastically smoothed H fields.

6.1.1. *Effects of topography.* Considering the two smoothed topographic fields shown in Figures 10 and 11 and then taking into account the further smoothing implicit in the finite-difference scheme, it is not surprising that the topographic effects resulting from this approach are relatively small. Using 1 December 1961 as an example, Figure 12 shows the 12-hour rainfall distribution between 06 GMT and 18 GMT on that day. Figure 13 shows the forecast rainfall totals for the period, which were obtained from the basic formulation and initial data for 00 GMT on 1 December 1961, and Figure 14 shows the forecast totals

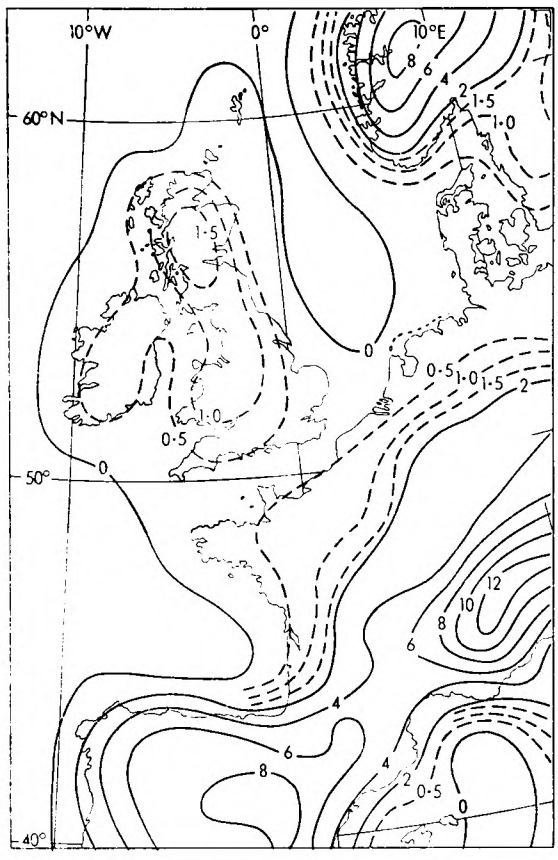

FIGURE 10. Moderately smoothed topographic field (units of 100 m)

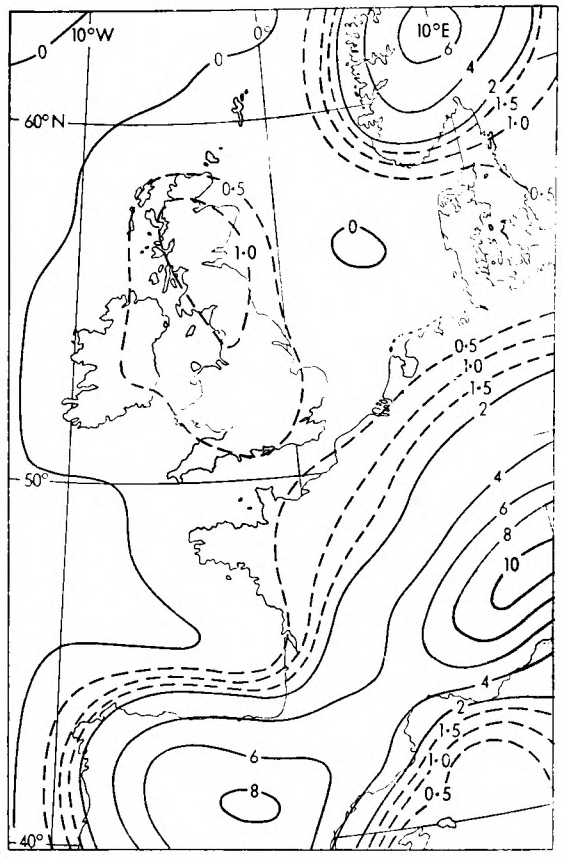

FIGURE 11. Drastically smoothed topographic field (units of 100 m)

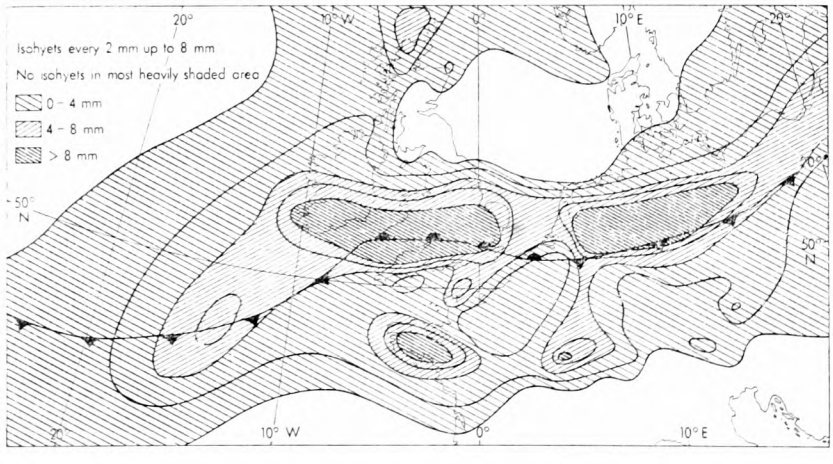

FIGURE 12. Estimated total rainfall for 06–18 GMT on 1 December 1961 based on reported totals

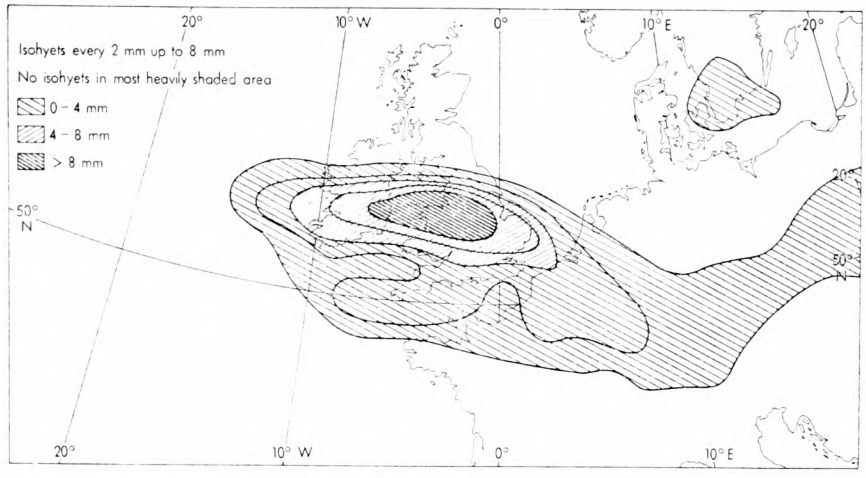

FIGURE 13. Forecast total rainfall for 06–18 GMT on 1 December 1961 obtained using basic formulation of 10-level model

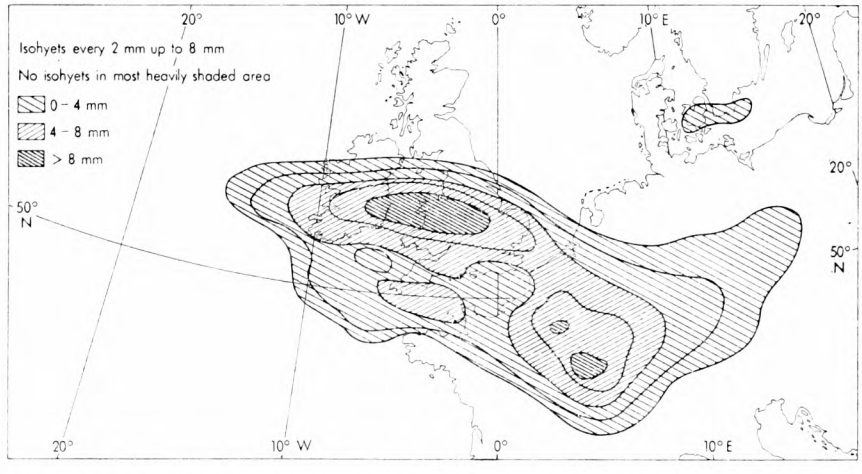

FIGURE 14. Forecast total rainfall for 06–18 GMT on 1 December 1961 from formulation of 10-level model which includes effects of topography

when topography was included. There have been some changes and they appear to be for the better. In general the rainfall was increased by several per cent over windward slopes and decreased slightly to leeward of the high ground. There was not much change in the forecast general motion of the depression, though slight filling of the centre occurred as the depression moved over land. The effects in the neighbourhood of the Alps are more apparent; there was some ridging of the contour pressure pattern over windward slopes and there was on this date a lee-trough development in the forecast fields (see Figure 15). There was also some diversion of the airflow around the high ground on windward slopes whilst the wind direction was more nearly down the slopes on the leeward sides of the Alps (see Figure 16). The forced vertical velocities were of the order of 10–20 mb/h up the windward slope and 20–30 mb/h down the leeward slope; at these levels such motions correspond to about 2–5 cm/s and 5–8 cm/s respectively. Having achieved a formulation

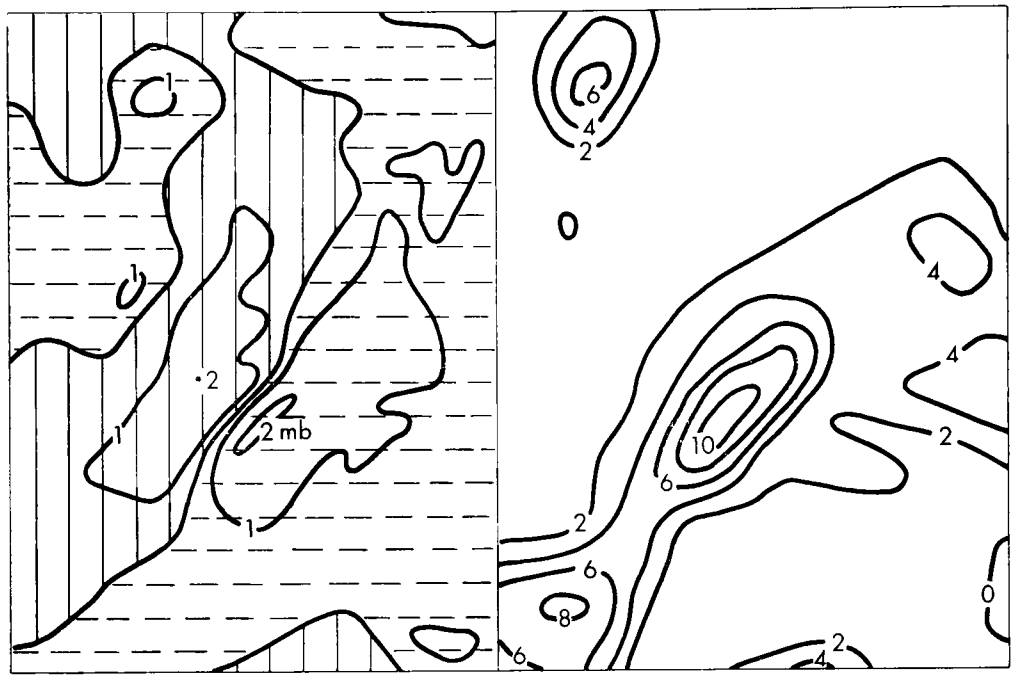

(*a*) Change in 12-hour forecast pressure for 12 GMT on 1 December 1961 due to inclusion of topography
— — Lower pressure | | | Higher pressure

(*b*) Smoothed topography field corresponding to area in (*a*)
Contours at intervals of 200 m.

FIGURE 15.

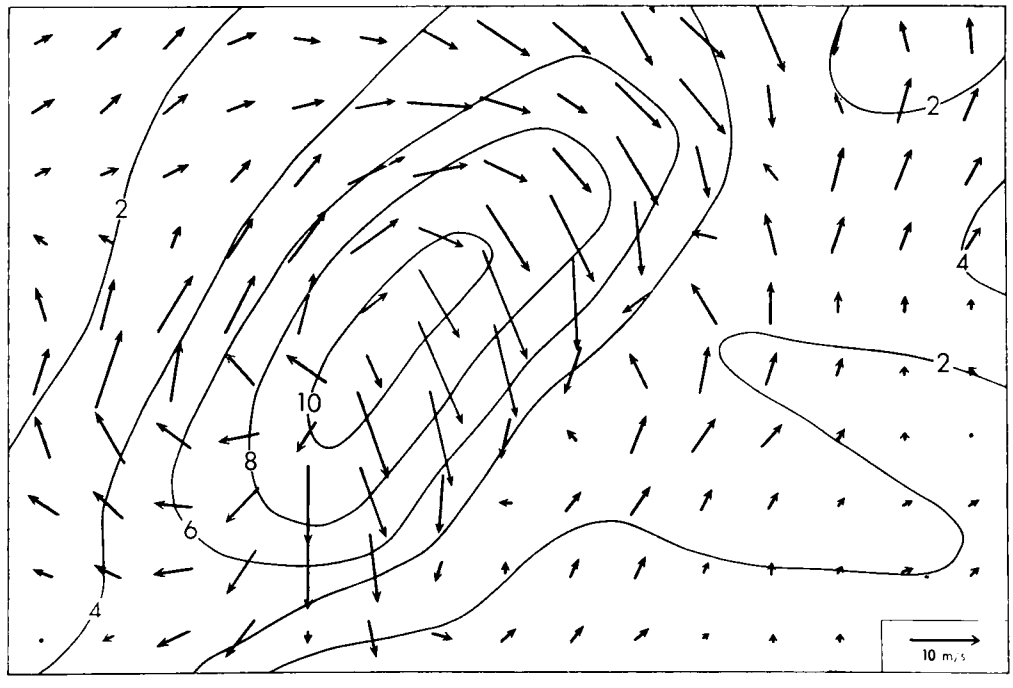

FIGURE 16. Change in 12-hour forecast 1000-mb wind for 12 GMT on 1 December 1961 due to inclusion of topography

Topography indicated by contours at intervals of 200 m.

which could be justified as an improvement to the forecast and also one which did not appear to lead to computational instability, attention was next directed to the problem of incorporation of surface friction.

6.2 *Friction*

In the real atmosphere the effects of the surface boundary layer are usually regarded as being confined to a layer about one kilometre thick and the fine structure of the surface friction effects, for example, can only be studied by considering many levels in this layer. In attempting to simulate surface friction effects in the 10-level model atmosphere it is obvious that only a crude representation is possible since the vertical resolution of the model provides only two levels, 1000 mb and 900 mb, in which to accommodate these effects.

The frictional effects which it was considered desirable to incorporate are

(i) the backing and weakening of the surface winds, and
(ii) the dynamic effects, i.e. the effects caused by frictional convergence or divergence which results from the forced vertical motions.

The latter effects were regarded as being the more important since among them are included the filling of depressions and the retardation in the movement of pressure systems generally. By making a decision to concentrate on simulating the dynamical effects it was appreciated that as a consequence it would only be possible to obtain a poor representation of the first effects.

The value of the horizontal stress vector at the surface has been taken to be equal to $\boldsymbol{\tau}_{1000}$, the value at 1000 mb. Further, if it is assumed that the friction layer does not extend above 900 mb, it is reasonable to make $\boldsymbol{\tau} = 0$ at 900 mb in the model atmosphere. The motion in the lowest layer of the model atmosphere can be represented by the equation

$$\frac{\mathrm{d}\mathbf{V}}{\mathrm{d}t} = -f\mathbf{k}\times\mathbf{V} - g\nabla h - g\frac{\partial\boldsymbol{\tau}}{\partial p}, \qquad \ldots (30)$$

i.e. the normal equation of motion with an additional, frictional, term added.

To represent $\partial\boldsymbol{\tau}/\partial p$ in the finite-difference approximation for equation (30), a one-sided difference is used at 1000 mb ($\boldsymbol{\tau}_{1000}/100$), a centred difference at 900 mb ($\boldsymbol{\tau}_{1000}/200$), and the term is zero at 800 mb and at the other pressure levels.

Krishnamurti[11] represents friction in his multi-level primitive equation model by a force in the opposite direction to that of the 1000-mb wind ($\mathbf{V}_{1000}$) and proportional to V^2_{1000}. Similar assumptions are made in the 10-level model, and the magnitude of the stress at 1000 mb is written $\tau_{1000} = \rho_{1000} C_D V^2_{1000}$. It remains to determine satisfactory values for the drag coefficient C_D. Even if it were possible to find and use a real value of C_D this would not give the correct backing and weakening of the model's 1000-mb wind because a one-sided difference is used to evaluate $\rho\partial\tau/\partial p$ and therefore this expression will be much smaller than the actual local value near the ground in the real atmosphere. The forced vertical velocities will be approximately correct since, as Sawyer[13] shows, these depend only upon the field of surface stress $\boldsymbol{\tau}_{1000}$. In fact the increment in $\mathrm{d}p/\mathrm{d}t$ due to friction across the layer affected by friction is

$$\Delta\omega_{\text{forced}} = \frac{g}{f}\left[\frac{\partial}{\partial y}\left\{(\tau_X)_{1000}\right\} - \frac{\partial}{\partial x}\left\{(\tau_Y)_{1000}\right\}\right], \qquad \ldots (31)$$

where $(\tau_X)_{1000}$, $(\tau_Y)_{1000}$ are the horizontal components of $\boldsymbol{\tau}_{1000}$ in the x and y directions.

6.2.1. *Drag coefficient over the sea, C_S.* After an examination of the available literature, Deacon[14] put forward the formula $C_{10} = (1{\cdot}10 + 0{\cdot}04V_{10}) \times 10^{-3}$ for the drag coefficient appropriate to the 10-m wind measurement in metres per second for land-locked sea areas. The formula was applicable to winds $V_{10} < 14$ m/s, and Deacon suggested a 20 per cent reduction as being a suitable drag coefficient for open sea areas. Since in the 10-level model to keep the problem simple, it is intended to discriminate between sea and land areas only and since some of the 'technically' sea areas will involve part land then a reasonable formula for a first approximation would be a 10 per cent reduction, i.e.

$$C_{10} = (1{\cdot}00 + 0{\cdot}036V_{10}) \times 10^{-3}.$$

Findlater *et alii*[15] have analysed data from Ocean Weather Stations 'I' and 'J' and classified these according to 900-mb wind speed and lapse rate. The data from the neutral lapse rate class of Table VII of their paper have been used to obtain Table II relating V_{10} to V_{900}. By equating V_{900} to the V_{1000} of the model it is possible to use the approximate formula above, appropriately corrected for direction, to construct a table of drag coefficient $C_D = C_S$, appropriate to the model's 1000-mb wind.

TABLE II. *The drag coefficient over the sea, C_S, appropriate to the 10-level model, as a function of the model's 1000-mb wind*

V_{900} speed category* *kt*	V_{10}/V_{900}	Corresponding average V_{1000} in 10-level model *m/s*	C_S *units of* 10^{-3}
10–19	0·85	7·7	0·89
20–29	0·77	12·9	0·80
30–39	0·71	18·0	0·73
40–49	0·67	23·2	0·70
⩾50	0·64	28·3 (corresponding to 55 kt)	0·67

* From Findlater *et alii*.[15]

In view of the approximations made, the neglect of variation of C_S with lapse rate, errors due to lack of wind data over sea, and lack of knowledge of the behaviour of C_S at high wind speeds, it was decided to reject a formula for use with the 10-level model in which there is a linear variation with wind speed and to use a constant value of C_S. Also since the greatest effect is at high wind speeds, a value appropriate to the higher wind speeds was selected, namely $0{\cdot}7 \times 10^{-3}$ for C_S. (At still higher wind speeds wave tops become sheared off and the drag coefficient is reduced; Deacon's[14] formula applies for surface winds of up to 14 m/s and thus for high speeds the value of C_D deduced from the approximate formula above is likely to be too great.)

6.2.2. *Drag coefficient over land, C_L.* Over land areas, topography and surface roughness are the main factors determining C_L, and lapse rate, which has a large diurnal variation, has been regarded as relatively less important. Only a rough approximation for C_L is feasible and a formula

$$C_L = (1.0 + 0{\cdot}0025H) \times 10^{-3}$$

is used, H being the height of topography above MSL, the same field values as used in representing topographic effects. It is a smoothed field and should avoid giving rise to

features of short wavelength which can become computationally unstable. Furthermore, the change from sea to land will be small and fairly smooth.

Cressman[16] regards C_L as being comprised of a constant, for which he uses a value of $1{\cdot}2 \times 10^{-3}$, plus a measure of the form drag; to estimate the form drag over high ground and mountains he uses a theoretical argument put forward by Sawyer.

Findlater *et alii*[15] have also analysed wind data for London/Heathrow Airport and Leuchars and determined an average value of the ratio of V_{surface} to V_{gradient} of 0·4 and an average angle of backing from geostrophic of 20°. Sawyer[13] and Cressman[16] both give tables of drag coefficients obtained from other workers and Table III is a selection of these, converted to give the equivalent C_L.

TABLE III. *Drag coefficient over land, C_L, for various areas*

Author	C_L *units of* 10^{-3}	Area
Sutcliffe (1936)	0·9	England
Lettau (1950)	1·3	Leipzig
Lettau (1957)	1·0	O'Neill, Nebraska
	2·8	Northern Germany
	1·9	Munich Forest
	3·8	Mountains, east Siberia

Pasquill[17] gives values of drag coefficient for various types of surface, and the equivalent C_L are given in Table IV.

TABLE IV. *Drag coefficient over land, C_L, for various types of surface**

C_L *units of* 10^{-3}	Underlying surface
0·126	mud flats, ice
0·22	level desert
0·28	lawn grass, 1 cm high
0·50	lawn grass, 5 cm high
0·87	grass, 60 cm high
1·3	fully grown root crops

* After Pasquill.[17]

These values would imply that the minimum value of C_L of $1{\cdot}0 \times 10^{-3}$ is too high. However, as Sutcliffe[18] pointed out the form drag due to one tree is comparable to the drag of an area of grassland one hundred times as large, and the effect of trees and buildings is difficult to assess. For land at height $H = 100$ m, C_L will be $1{\cdot}25 \times 10^{-3}$, which agrees well with the values in Table III. For high mountains, such as the Alps, form drag has been deduced from Sawyer's calculations using an efficiency factor of about $\frac{1}{4}$, to give qualitative agreement with the formula, though naturally when large values of H are concerned further research is necessary before confidence can be placed in the C_L formulation.

6.2.3. *Effects due to friction.* The difference which the incorporation of friction makes to the forecast fields is quite interesting. Figures 17 and 18 show the differences in the 12-hour and 24-hour forecasts, from initial data at 00 GMT on 1 December 1961, of the ω_{900} field, which result from incorporating frictional terms in the equations of motion. Analyses taken from the charts of the Central Forecasting Office, Bracknell, have been

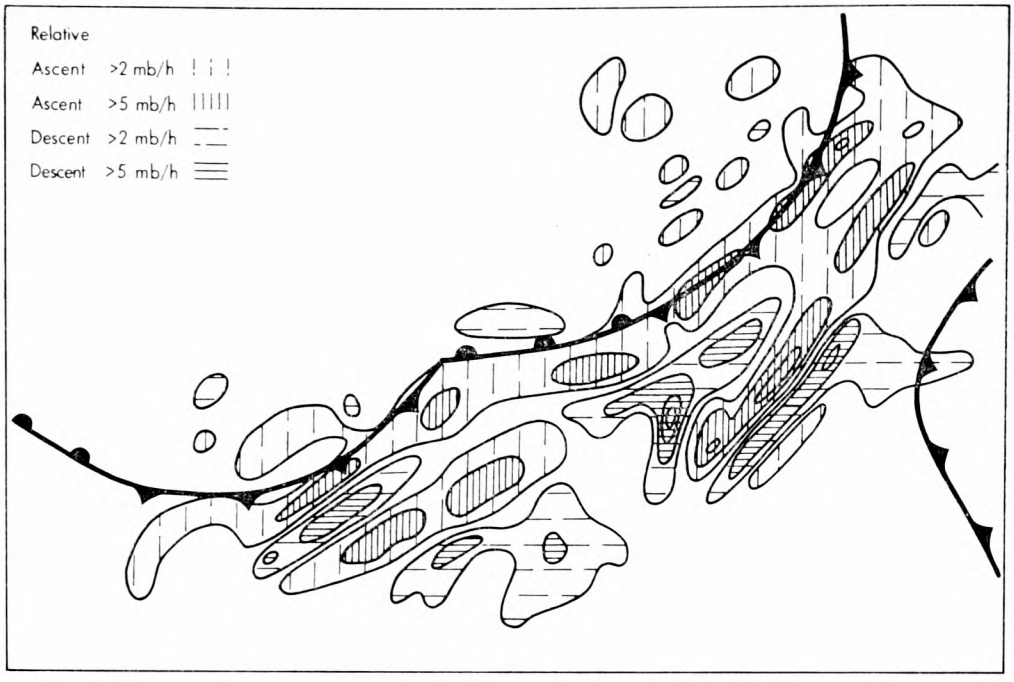

FIGURE 17. Difference in 12-hour forecast ω_{900} field for 12 GMT on 1 December 1961 due to incorporation of friction
Subjective frontal analysis of the Central Forecasting Office, Bracknell, superimposed.

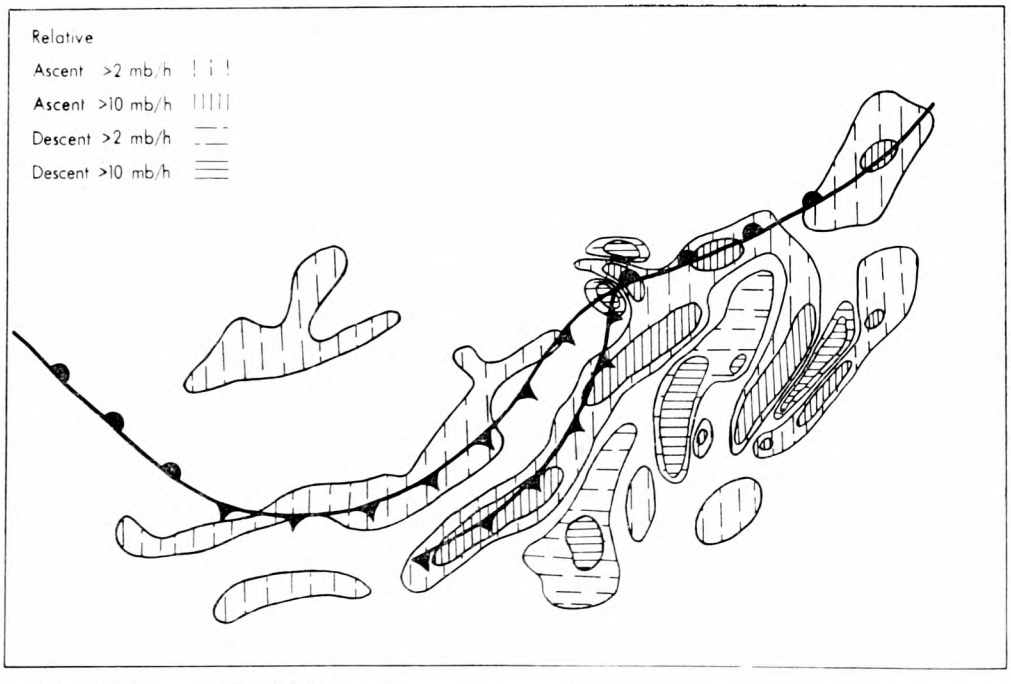

FIGURE 18. Difference in 24-hour forecast ω_{900} field for 00 GMT on 2 December 1961 due to incorporation of friction
Subjective frontal analysis of the Central Forecasting Office, Bracknell, superimposed.

superimposed on the appropriate charts and it is noticeable that the regions of maximum change in ω_{900} are closely identifiable with frontal positions. It is also of interest that although it was considered reasonable to drop one front at 12 GMT on 1 December 1961 it had to be reintroduced at 00 GMT on 2 December 1961. Figures 17 and 18 suggest that the fronts were still identifiable at both times although at the 24-hour forecast stage the more northerly of the two fronts was apparently a weaker feature.

Figure 19 shows that the dynamical effects resulting from the inclusion of the frictional terms are quite considerable. In this case the filling of the storm centre between 00 GMT and 12 GMT on 26 December 1960 was correctly predicted when frictional terms were incorporated, although with earlier formulations excessive deepening had been predicted.

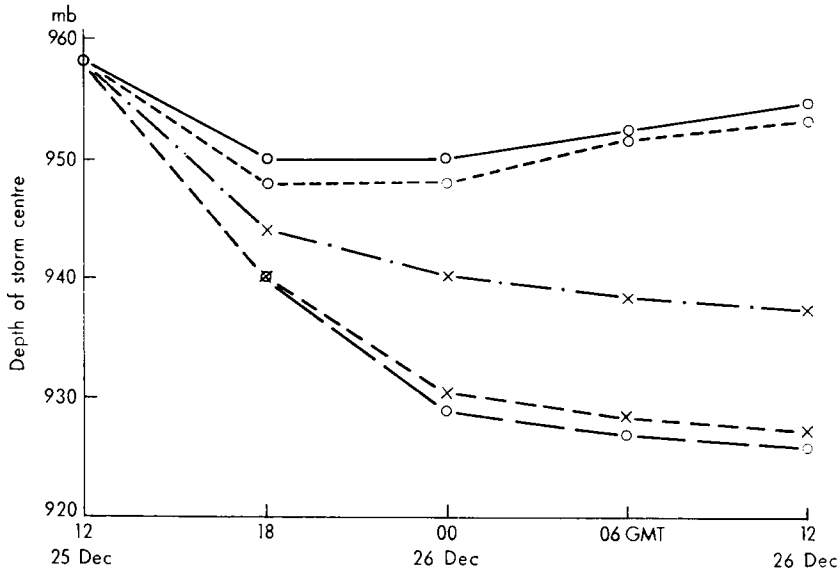

FIGURE 19. Depth of storm centre (actual and forecast) at 6-hour intervals from 12 GMT on 25 December 1960

o——o Actual from Central Forecasting Office, Bracknell, charts
×---× Forecast from basic formulation of 10-level model
o— —o Forecast incorporating convective adjustments
×—·—× Forecast incorporating convective adjustments, topography and lateral diffusion
o- - -o Forecast incorporating convective adjustments, topography, lateral diffusion and friction

6.3. *Horizontal diffusion*

Horizontal diffusion terms are included in the prediction equation for two reasons. Firstly, it is desirable to introduce into the formulation a representation of the redistribution of certain physical quantities in the real atmosphere by turbulent eddies smaller than those which can be represented by the basic reference grid. Secondly, it is equally desirable to include horizontal diffusion in each of the non-linear equations as a safeguard against non-linear computational instability. It can be argued that the present difference scheme outlined in Section 4 imposes no direct smoothing of high wave numbers unless the diffusion terms are included and therefore large truncation errors may occur in the absence of such terms because the grid system is incapable of resolving wavelengths appropriate to the high wave numbers.

Since the diffusion term is computed by a forward time-step of $2\delta t$ and the basic grid length over which the diffusion term is calculated is $2a$, it is convenient in the ensuing section to write $\delta t'$ in place of $2\delta t$ and a' in place of $2a$.

The role of the diffusion term can be examined by considering equation

$$F_t = K(F_{xx} + F_{yy}).$$

Substituting $F = G(t)\, e^{i(\lambda x + \mu y)}$, where λ, μ are wave numbers ($\lambda = 2\pi/L_x$, $\mu = 2\pi/L_y$ and L_x, L_y are wavelengths), and introducing finite differences with a forward time-step $\delta t'$, then

$$F(t+\delta t') = F(t) + K\nabla^2 F\delta t'.$$

Thus
$$G(t+\delta t') = G(t)\left[1 - 4K\delta t'\left\{\frac{\sin^2\left(\frac{\lambda\delta x'}{2}\right)}{(\delta x')^2} + \frac{\sin^2\left(\frac{\mu\delta y'}{2}\right)}{(\delta y')^2}\right\}\right].$$

For the shortest possible waves $L_x = 2\delta x'$, $L_y = 2\delta y'$, and

$$G(t+\delta t') = G(t)\left[1 - \frac{8K\delta t'}{(a')^2}\right]$$

where
$$\left[1 - \frac{8K\delta t'}{(a')^2}\right]$$

represents a damping factor which is applied to the amplitude of the wave.

Since a value of $K = 10^5$ m^2/s is used in the main part of the computation area away from the control zone with a value of $\delta t' = 180$ s and $a' = 109$ km, this means that waves of double grid-length, $4a$, are damped by e^{-1} of their amplitude in just over 4 hours, whilst in the boundary zone where $K = 10^6$ m^2/s the equivalent damping effect is achieved in approximately 25 minutes.

A physical interpretation of the value of the coefficient of lateral diffusion is possible through the classical mixing-length theory. The coefficient has the dimensions of a length times a velocity. In the mixing-length theory the coefficient is taken to be the product of a length equal to the scale of the eddies, by virtue of which the diffusion is assumed to operate, and a velocity equal to that of the eddy motion relative to the mean flow. For example, the value of $K = 10^5$ m^2/s is equivalent to diffusion through eddies with path lengths 10 km and characteristic velocities of 10 m/s.

6.3.1. *Effects of inclusion of diffusion terms.* The inclusion of the diffusion term in each of the non-linear equations has resulted in removing the small roughnesses which were apparent in the 24-hour forecasts, without producing any significant effect in the synoptic-scale features. Twelve-hour forecasts for 25 December 1960, however, show that the main low-pressure centre is about 10 mb lower when lateral diffusion terms are excluded than when they are included (see Figure 19), the latter seemingly more correct.

A further advantage of including diffusion terms is their indirect damping of the inertio-gravitational waves which result from imperfectly balanced initial conditions. There was a small residual gravity wave even when the initial winds were obtained by solving the modified balance equation as suggested in a paper by Benwell and Bretherton.[5] This undesirable wave was amplified after topography was incorporated into the model, but

inclusion of diffusion terms almost completely eliminated it. Figure 20 illustrates the damping by comparing the variation of the mean height field of the 1000-mb pressure level during the course of a 24-hour forecast with and without both lateral diffusion and convective adjustment.

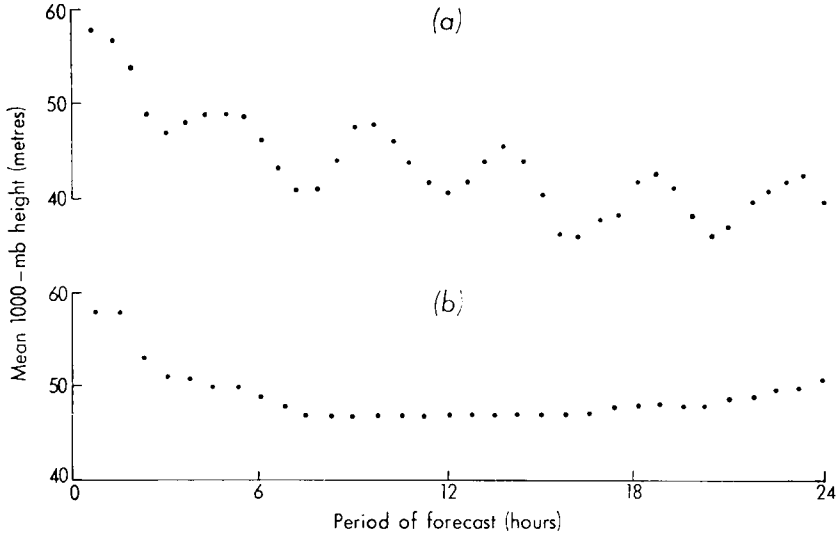

FIGURE 20. Variation of mean height of 1000-mb surface over computation area during a forecast period of 24 hours

(*a*) Without lateral diffusion (*b*) With lateral diffusion
That part of the area within 300 km of the lateral boundaries was excluded.
Initial data 00 GMT on 1 December 1961.

From experiments mentioned earlier in this section (6.1.) it was noted that in the absence of lateral diffusion it appeared to be necessary to use drastically smoothed H fields. Following the incorporation of lateral diffusion another series of experiments was carried out using as alternatives the moderately smoothed and the unsmoothed fields of H. From these experiments it appeared to be perfectly safe to use the moderately smoothed fields of H and it is also thought that no instabilities would result from using an unsmoothed H field, although in this case very large vertical velocities may have to be accepted in the immediate vicinity of the Alps, and to a lesser extent over the Pyrenees and the Norwegian mountain ranges. However, as a safeguard against undesirable growth of gravity waves which result from the rougher topographic field, a non-linear coefficient of lateral diffusion was tried which gave a highly selective damping of short waves whilst leaving the synoptic-scale features virtually unchanged. The non-linear coefficient of diffusion was included by replacing K by $K^\circ|\nabla^2|$. K° is chosen so that a wave of double grid-length is damped to e^{-1} of its original amplitude in the same time with non-linear diffusion as with linear diffusion: note that K° is proportional to the amplitude of the wave being diffused.

The results of some 24-hour forecasts with linear and non-linear coefficients of diffusion are summarized in Figure 21, which shows the maximum vertical velocity near the Alps throughout the forecast period. It is clear from this diagram that the use of the non-linear coefficient of diffusion makes little difference in this case, although it is as well to have such a scheme in reserve.

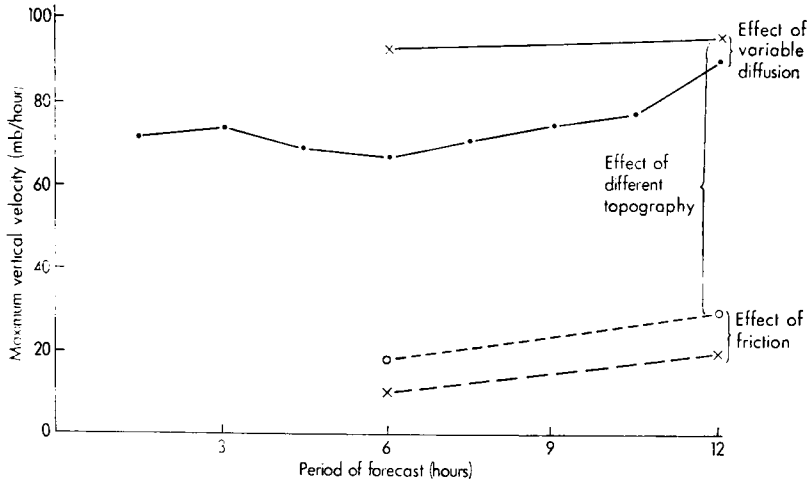

FIGURE 21. Changes in maximum vertical velocity in the vicinity of the Alps during a 24-hour forecast due to changes in incorporated diffusion, topography and friction

·——· Rough topography, non-linear diffusion, no friction
×——× Rough topography, linear diffusion, no friction
o- - -o Moderately smoothed topography, linear diffusion, no friction
×— —× Moderately smoothed topography, linear diffusion, friction

7. CONDENSATION AND EVAPORATION

7.1. *Introduction*

The general procedure by which values of the dependent variables at time $t+2\delta t$ are calculated from those at time t has been outlined in Section 4. In this section the procedures for calculating the contributions to Q and W (see equations (4) and (6)) from the condensation of water vapour and the evaporation of rainfall are described. No account of the ice phase is at present included in the model. It is necessary to test each 100-mb layer (below 300 mb) for saturation with respect to liquid water and this is done by comparing the humidity mixing ratio, r, representative of a layer with the appropriate saturation mixing ratio, r_s. This saturation mixing ratio is obtained using an empirically determined quartic polynomial in the thickness, h', of the layer. Different polynominal coefficients are, of course, required for each of the seven layers for which humidity mixing ratios are predicted, so that, in all, 35 constants must be stored. A high degree of accuracy is attained with this method of calculating r_s, provided that h' is sufficiently large. If h' becomes smaller than some critical value (different for each layer), r, r_s and X (large-scale relative humidity) are all taken to be zero in the layer concerned.

The original formulation of the 10-level model, described by Bushby and Timpson,[4] differed from that described here in that terms accounting for condensation of water vapour and evaporation of rainfall were included in the thermodynamic and hydrological equations for both the forward and the centred time-steps. In the present formulation, values of the dependent variables at $t+2\delta t$ are first obtained with no account being taken of condensation or evaporation, and these effects are then represented by adjustments to the thicknesses and humidity mixing ratios where necessary.

A number of successful rainfall predictions were computed using the original formulation, but eventually a serious defect became apparent. At each grid point for which $\partial h'/\partial t$ and $\partial r/\partial t$ were to be calculated at time t, it was necessary to decide whether the air was saturated or not. The finite-difference scheme (described in Section 4) is such that this decision was inevitably based on a comparison of the mean of the four surrounding humidity mixing ratios with the saturation mixing ratio corresponding to the mean of the four surrounding thicknesses. As a result, the procedure appropriate to saturated air was unlikely to be adopted in integrating from t to $t+\delta t$ unless the air at all four surrounding grid points was saturated at time t, and the procedure appropriate to unsaturated air therefore tended to be applied in regions where the air was saturated. This was especially the case in frontal zones, where, normal to the front, the horizontal extent of regions of saturated air is only a few grid lengths. It was found that marked supersaturations, with relative humidities up to 150 per cent, developed in this way, and there were corresponding deficiencies in forecast rainfall amounts.

This original formulation was therefore superseded by one which was essentially similar to that described below, but which retained the stringent assumptions regarding the evaporation of rainfall implicit in the original scheme. These assumptions were that liquid water falling into an unsaturated layer evaporates immediately until either it is exhausted or the layer becomes saturated. More recently an improved treatment of the evaporation of rainfall has been formulated, and it is this which is described in Section 7.3.

Three assumptions which are implied in the formulation may be noted:

(i) No condensation of water vapour takes place as a result of large-scale motions (as distinct from small-scale convective motions, see Section 9.2.) until air becomes saturated on the grid scale.

(ii) Condensation of water vapour takes place at a sufficient rate to keep the air exactly saturated whenever supersaturation would otherwise occur.

(iii) There is no storage of liquid water in the model atmosphere, so that any liquid water produced as a result of condensation falls immediately through the layers below, is modified by evaporation if any of these layers is unsaturated, and may reach the 1000-mb level where it is interpreted as surface rainfall distributed over the preceding double time-step.

7.2. *The condensation of water vapour*

Suppose that $[r]_{k+\frac{1}{2}}$ and $[h']_{k+\frac{1}{2}}$ are the humidity mixing ratio and the thickness of layer $k+\frac{1}{2}$ obtained at time $t+2\delta t$ with no account taken of condensation and evaporation during the time interval $(t, t+2\delta t)$ and that $[r_s]_{k+\frac{1}{2}}$ is the saturation mixing ratio obtained from $[h']_{k+\frac{1}{2}}$ using the appropriate quartic polynomial. If $[r]_{k+\frac{1}{2}} \leqslant [r_s]_{k+\frac{1}{2}}$ no action is taken. If, however, $[r]_{k+\frac{1}{2}} > [r_s]_{k+\frac{1}{2}}$, adjusted values $r_{k+\frac{1}{2}}$, $h'_{k+\frac{1}{2}}$ are obtained such that $r_{k+\frac{1}{2}} = (r_s)_{k+\frac{1}{2}}$ where $(r_s)_{k+\frac{1}{2}}$ is the saturation mixing ratio corresponding to $h'_{k+\frac{1}{2}}$. In order to take account of the effects of latent-heat release on the thickness of the layer, $r_{k+\frac{1}{2}}$ and $h'_{k+\frac{1}{2}}$ are obtained by solving simultaneously the following pair of equations:

$$c_p(T_{k+\frac{1}{2}}-[T]_{k+\frac{1}{2}}) = L([r]_{k+\frac{1}{2}}-(r_s)_{k+\frac{1}{2}}), \qquad \ldots (32)$$

$$\frac{(r_s)_{k+\frac{1}{2}}-[r_s]_{k+\frac{1}{2}}}{T_{k+\frac{1}{2}}-[T]_{k+\frac{1}{2}}} = \frac{\epsilon L[r_s]_{k+\frac{1}{2}}}{R[T]^2_{k+\frac{1}{2}}}, \qquad \ldots (33)$$

where $[T]_{k+\frac{1}{2}}$ and $T_{k+\frac{1}{2}}$ are the values of the temperature of the layer at $t+2\delta t$ before and after adjustment respectively. The first of these equations describes the conservation of heat during the condensation and the second is a finite-difference representation of the Clausius-Clapeyron equation. $T_{k+\frac{1}{2}}$ and $[T]_{k+\frac{1}{2}}$ are related to $h'_{k+\frac{1}{2}}$ and $[h']_{k+\frac{1}{2}}$ by equations of the form

$$T_{k+\frac{1}{2}} = gh'_{k+\frac{1}{2}}/R \ln\left(\frac{k+1}{k}\right). \quad \ldots (34)$$

The elimination of $(r_s)_{k+\frac{1}{2}}$ from equations (32) and (33) and the substitution of thicknesses for temperatures gives the relationship

$$h'_{k+\frac{1}{2}} = [h']_{k+\frac{1}{2}} + \frac{R\ln((k+1)/k)}{g} \frac{L\{[r]_{k+\frac{1}{2}} - [r_s]_{k+\frac{1}{2}}\}}{c_p + \dfrac{\epsilon L^2 R\{\ln((k+1)/k)\}^2 [r_s]_{k+\frac{1}{2}}}{g^2 [h']^2_{k+\frac{1}{2}}}}. \quad \ldots (35)$$

The adjusted humidity mixing ratio $r_{k+\frac{1}{2}} = (r_s)_{k+\frac{1}{2}}$ is then obtained from $h'_{k+\frac{1}{2}}$ using the quartic polynomial. The mixing ratio of liquid water produced in layer $k+\frac{1}{2}$ as a result of the condensation is $[r]_{k+\frac{1}{2}} - (r_s)_{k+\frac{1}{2}}$, and, if M_k is the mixing ratio of liquid water transferred from layer $k-\frac{1}{2}$ to layer $k+\frac{1}{2}$ during the time interval $(t, t+2\delta t)$,

$$M_{k+1} = M_k + [r]_{k+\frac{1}{2}} - (r_s)_{k+\frac{1}{2}}.$$

7.3. *The evaporation of rainfall*

The mixing ratio M_k g/kg of liquid water falling through level k during $2\delta t$ seconds is equivalent to a rate of rainfall P_k mm/h given by

$$P_k = 10\frac{b}{g}M_k \frac{3600}{2\delta t}, \quad \ldots (36)$$

where $b/g = 1/9{\cdot}8$ is the mass of a 100-mb layer of air in kilogrammes per square centimetre. If $[r]_{k+\frac{1}{2}} < [r_s]_{k+\frac{1}{2}}$, some or all of this rainfall will evaporate as it falls through layer $k+\frac{1}{2}$.

By assuming that departures of the 10-level model atmosphere from the ICAO Standard Atmosphere do not significantly influence the evaporation process, it is possible to rewrite the semi-empirical evaporation formula of Best[19] in the form

$$a_k^2 - a_{k+1}^2 = E_{k+\frac{1}{2}}(1 - X_{k+\frac{1}{2}})^{1.13}, \quad \ldots (37)$$

where a_k and a_{k+1} are the radii (in millimetres) of raindrops at levels k and $k+1$ respectively. $E_{k+\frac{1}{2}}$ is a constant for each layer of the model atmosphere and is given by

$$E_{k+\frac{1}{2}} = 1{\cdot}375\{\exp[-0{\cdot}29(h_{\mathrm{ICAO}})_{k+1}] - \exp[-0{\cdot}29(h_{\mathrm{ICAO}})_k]\},$$

where $(h_{\mathrm{ICAO}})_k$ and $(h_{\mathrm{ICAO}})_{k+1}$ are the heights in kilometres of levels k and $k+1$ in the ICAO Standard Atmosphere.

Two further assumptions are now made:

(i) The raindrop size distribution is related to the rate of rainfall by the empirical formula of Best[20] and therefore has a median volume radius given by

$$a_k = 0{\cdot}55P_k^{0{\cdot}232}. \quad \ldots (38)$$

(ii) The effects of evaporation on the drop size distribution are such that the radius a_{k+1} obtained from a_k by using equation (37) is the median volume radius of the distribution at level $k+1$, and that this distribution is again given by Best's formula, so that

$$P_{k+1} = (1{\cdot}82a_{k+1})^{4{\cdot}31}. \quad \ldots (39)$$

Equations (36), (37), (38) and (39) are used to calculate M_{k+1}, and the adjusted variables $r_{k+\frac{1}{2}}$, $h'_{k+\frac{1}{2}}$ are then given by

$$r_{k+\frac{1}{2}} = [r]_{k+\frac{1}{2}} + M_k - M_{k+1}, \quad \ldots (40)$$

$$h'_{k+\frac{1}{2}} = [h']_{k+\frac{1}{2}} - \frac{R\ln((k+1)/k)}{g}\frac{L}{c_p}(M_k - M_{k+1}). \quad \ldots (41)$$

If a^2_{k+1} given by equation (37) is negative, M_{k+1} is taken to be zero; that is, all the liquid water falling through level k is assumed to evaporate in layer $k+\frac{1}{2}$. If $r_{k+\frac{1}{2}}$ and $h'_{k+\frac{1}{2}}$ obtained from equations (40) and (41) are such that $r_{k+\frac{1}{2}} > (r_s)_{k+\frac{1}{2}}$, a second solution is obtained such that $r_{k+\frac{1}{2}} = (r_s)_{k+\frac{1}{2}}$. The required thickness is now given by equation (35), where in this case $[r]_{k+\frac{1}{2}} - [r_s]_{k+\frac{1}{2}} < 0$.

8. SURFACE EXCHANGES OF SENSIBLE AND LATENT HEAT

8.1. *Introduction*

A number of successful 24-hour forecasts have been computed using versions of the 10-level model which neglect the effects of sensible- and latent-heat exchanges between the atmosphere and the underlying surface. Nevertheless, such surface exchanges are important in the context of this model, because of their link with small-scale convection and the associated convective rainfall, and also because on some occasions the transfer of heat from the surface significantly influences the development of the large-scale flow.

For the purposes of the 10-level model the fluxes of sensible heat and water vapour at the earth's surface have been expressed, in a manner analogous to the bulk aerodynamic equations (Roll,[21] p. 252), as

$$F_H = \rho_{1000} k_E V_{1000} c_p \Delta T, \quad \ldots (42)$$

$$F_W = \rho_{1000} k_E V_{1000} \Delta r, \quad \ldots (43)$$

where $\Delta T = T_0 - T_{950} - gh'_{950}/2c_p$, $\Delta r = r_0 - r_{950}$, and T_{950} is the temperature derived from h'_{950} by using the formula

$$T_{950} = gh'_{950}/R\ln(10/9). \quad \ldots (44)$$

The ICAO Standard Atmosphere 1000-mb density is used throughout for ρ_{1000}.

The model atmosphere is bounded below by the 1000-mb surface (see Section 2) and, consistent with this, the earth's surface has been regarded as coincident with the 1000-mb surface in formulating equations (42) and (43). These equations differ from the bulk aerodynamic equations in that, whereas the latter usually employ observations at the 10-m level, T_{950} and r_{950} are appropriate to a level $\frac{1}{2}h'_{950}$ ($\approx$450 m) above the surface. The configuration of the variables used in these equations is illustrated in Figure 22.

The balance of energy at the earth's surface is described by the equation

$$F_H + LF_W = R_N - F_G,$$

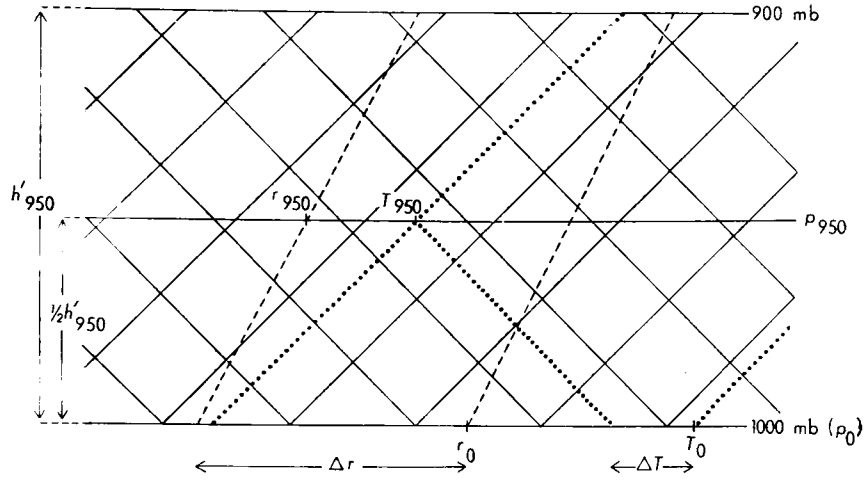

FIGURE 22. Tephigram illustrating the configuration of the variables used in the aerodynamic formulae for the surface fluxes

which it is convenient to write in the form

$$F_H + LF_W = (1-\mu)R_N, \qquad \ldots (45)$$

where $\mu = F_G/R_N$.

8.2. *The surface energy fluxes over the sea*

The large thermal capacity of the sea makes it possible to regard the sea surface temperature as constant in time over periods of several days. Furthermore, the humidity mixing ratio at the sea surface may be taken equal to the saturation mixing ratio r_s (T_0, p_0) corresponding to the sea surface temperature T_0 and the surface pressure p_0 (= 1000 mb). Thus with T_0 and r_0 constant during the course of a forecast, F_H and F_W may be calculated directly from equations (42) and (43). Monthly mean distributions of sea surface temperature are at present used.

The relationship between the exchange coefficient k_E appropriate to equations (42) and (43) and the coefficient k_a appropriate to the bulk aerodynamic formulae applied at the 10-m level, depends on the stratifications of temperature and humidity in the lowest few hundred metres of the atmosphere. Observations of these stratifications described by Craig[22] suggest the approximations $k_E = k_a$ for $\Delta T \geqslant 0$ and $k_E = 0{\cdot}1\, k_a$ for $\Delta T < 0$, and these have been adopted here.

In conditions of near-neutral stability the exchange coefficient $k_a = 1{\cdot}25 \times 10^{-3}$ is fairly widely accepted (Robinson[23]), but studies such as those of Manabe[24] show that k_a increases significantly with increasing sea–air temperature contrast. Accordingly values of the exchange coefficient given by

$$k_E = \begin{cases} (1{\cdot}25 + 0{\cdot}1\Delta T) \times 10^{-3} & \text{for } \Delta T \geqslant 0 \\ 0{\cdot}1(1{\cdot}25 + 0{\cdot}1\Delta T) \times 10^{-3} & \text{for } \Delta T < 0 \end{cases}$$

have been used in applying equations (42) and (43) over the sea.

8.3. *The surface energy fluxes over land*

Over land the direct application of the aerodynamic formulae is hindered by the rapid variations of surface temperature in response to diurnal variations in the net radiation

flux. A combined aerodynamic energy-balance approach analogous to that suggested by Penman[25] has been used, and the problem of determining F_H and F_W is treated in three parts: (i) the calculation of R_N, (ii) the calculation of F_G, and (iii) the partitioning of $R_N - F_G$ into F_H and LF_W.

(i) *The net radiation flux.* For cloudless skies Monteith and Szeicz[26] and others have shown empirically that the net vertical radiation flux at the surface, R_N, is linearly related to the vertical flux of incoming, direct plus diffuse, solar radiation, $SF' \sin\theta$, by the equation

$$R_N = \frac{1-\alpha}{1+\beta} SF' \sin\theta - L'_0, \qquad \ldots (46)$$

where α is the albedo of the land surface and β and L'_0 are constants of the regression interpreted as a heating coefficient and the long-wave radiation at zero insolation respectively. The transmission function

$$F' = 0{\cdot}6 + 0{\cdot}2 \sin\theta,$$

determined empirically by Lumb[27] for clear skies, has been used and $\sin\theta$ has been calculated from the formula

$$\sin\theta = \sin\delta \sin\phi - \cos\delta \cos\phi \cos\left(\frac{\pi t}{12} + \lambda\right)$$

where t is GMT in hours and δ, the solar declination, has been assigned monthly mean values. When the sun is below the horizon, that is, when $\sin\theta$ calculated from the above formula is negative, equation (46) is replaced by $R_N = -L'_0$.

It remains to account for the effects of cloud on the net radiation flux. Empirical relationships, similar to those described by Smagorinsky,[28] between the relative humidities predicted in the 300–500, 500–800 and 800–1000-mb layers of the model atmosphere and the observed fractional cloud cover in the high, medium and low cloud categories have been obtained from a limited investigation. These relationships are illustrated by Figure 23.

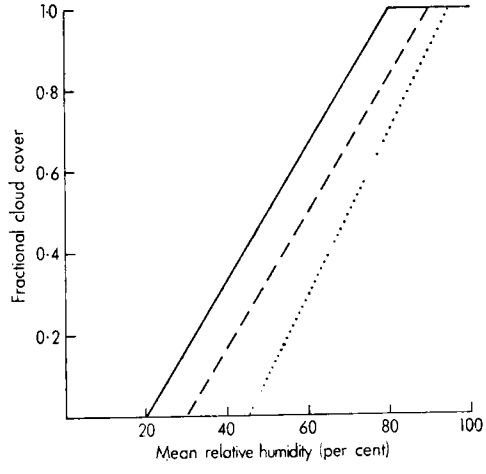

FIGURE 23. Relationship between predicted relative humidity and fractional cloud cover used in the 10-level model atmosphere

——— High cloud (300–500-mb layer) — — Medium cloud (500–800-mb layer)
. . . . Low cloud (800–1000-mb layer)

The effects of cloud on the net radiation flux R_N have been represented by replacing the clear-skies parameters F' and L'_0 by F and L_0 in equation (46) where

$$F = F'(1-0{\cdot}4c_h)(1-0{\cdot}7c_m)(1-0{\cdot}7c_l), \quad \ldots (47)$$

$$L_0 = L'_0(1-0{\cdot}1c_h-0{\cdot}3c_m-0{\cdot}6c_l), \quad \ldots (48)$$

where c_h, c_m, c_l are given by Figure 23. The values of the coefficients in equation (47) have been chosen to be broadly consistent with the observations of Robinson,[29] Monteith [30] and Lumb.[27] The form of equation (48) is that discussed by Kondrat'yev.[31]

(ii) *The heat flux into the ground.* During the day-time, F_G is generally a small term in equation (45) so that a fairly crude estimate of its value is adequate for the present purposes. On the basis of observations, such as those described by Brooks and Goddard,[32] two values, one for $R_N \geqslant 0$ and one for $R_N < 0$, of the parameter $\mu = F_G/R_N$ have been specified for use in equation (45).

(iii) *Partitioning the available energy into sensible and latent heat.* During the night the latent-heat flux into the atmosphere over vegetation is close to zero (see, for example, the results of Brooks and Goddard[32]); also, the contribution of dew formation to the surface energy balance has been neglected for the present. Accordingly for $R_N < 0$, the flux relationships $F_W = 0$ and $F_H = (1-\mu)R_N$ follow from equation (45).

For $R_N \geqslant 0$ a method analogous to that described by Penman[25] has been used to partition the energy flux $(R_N - F_G)$, which is available at the surface for transfer into the atmosphere, into sensible and latent heat. Approximating to r_0 in equation (43) by

$$r_0 = X_0\left((r_s)_{950} + (p_0 - p_{950})\left[\left(\frac{\partial r_s}{\partial p}\right)_T\right]_{950} + (T_0 - T_{950})\left[\left(\frac{\partial r_s}{\partial T}\right)_p\right]_{950}\right),$$

the troublesome surface temperature may be eliminated from equations (42) and (43) to obtain

$$LF_W = LF_W^* + X_0 q F_H, \quad \ldots (49)$$

where

$$F_W^* = \rho_{1000} k_E V_{1000}\left(X_0\left[(r_s)_{950} + (p_0 - p_{950})\left\{\left(\frac{\partial r_s}{\partial p}\right)_T\right\}_{950} + \frac{g}{c_p}\frac{h'_{950}}{2}\left\{\left(\frac{\partial r_s}{\partial T}\right)_p\right\}_{950}\right] - r_{950}\right),$$

and

$$q = \frac{L}{c_p}\left[\left(\frac{\partial r_s}{\partial T}\right)_p\right]_{950}.$$

Using the Clausius-Clapeyron equation and equation (44) it may be shown that

$$F_W^* = \rho_{1000} k_E V_{1000}\left\{X_0\left[A + \frac{B}{h'_{950}}\right](r_s)_{950} - r_{950}\right\}, \quad \ldots (50)$$

and

$$q = \frac{C}{(h'_{950})^2}(r_s)_{950},$$

where

$$A = 1 - \frac{(p_0 - p_{950})}{p_{950}}, \qquad B = \frac{R}{2c_p}\frac{\epsilon L\{\ln(10/9)\}^2}{g}, \qquad C = \frac{R}{c_p}\frac{\epsilon L^2\{\ln(10/9)\}^2}{g^2}.$$

Equations (45) and (49) may now be solved to give

$$F_H = \frac{(1-\mu)R_N - LF_W^*}{1+X_0 q}, \qquad \ldots (51)$$

$$LF_W = \frac{LF_W^* + X_0 q(1-\mu)R_N}{1+X_0 q}. \qquad \ldots (52)$$

Conditions at the surface are represented in equations (51) and (52) by the surface relative humidity X_0 only. Given this parameter, equations (50), (51) and (52) enable F_H and F_W to be calculated from variables available in the model atmosphere. The choice of the exchange coefficient k_E for use in equation (50) is a rather difficult matter; a relatively small value ($1{\cdot}25 \times 10^{-4}$) has been used so far, but it is expected that this will be modified in the light of experience.

(iv) *The surface parameters.* Four surface parameters, $(1-\alpha)/(1+\beta)$, L'_0, μ and X_0, are required for the calculation of F_H and F_W by the method described above. The values

$$\alpha = 0{\cdot}25,\ \beta = 0{\cdot}1,\ L'_0 = 0{\cdot}05\mathrm{S},\ \mu = \begin{cases} 0{\cdot}1 & \text{for } R_N \geqslant 0 \\ 0{\cdot}5 & \text{for } R_N < 0 \end{cases},\qquad X_0 = 0{\cdot}8,$$

have been used, and are representative of well-watered grass-covered surfaces (see Monteith and Szeicz[26] for α, β, and L'_0, and Szeicz *et alii*[33] for μ). In reality, of course, these parameters are functions of factors such as soil and vegetation type, snow cover and soil moisture deficit. A refined version of the representation described above, in which the surface parameters are specified as functions of climatic type, snow cover and the month of the year, has been formulated and will be incorporated into the model atmosphere in due course.

8.4. *Energy redistribution within the atmospheric boundary layer*

The transfer of heat and water vapour across the earth's surface has the effect in the model atmosphere of modifying the thickness and humidity mixing ratio of the lowermost 100-mb layer. The effects of the surface transfers may be confined to this layer, or, if the static stability permits, may be extended through two or more such layers by convective motions, including cumulus convection, on scales of up to a few kilometres, termed by Ludlam[34] 'small-scale convection'. The set of 100-mb layers adjacent to the surface which are modified in this way is referred to as 'the atmospheric boundary layer'. The effects of small-scale convection are represented in the model atmosphere by the convective adjustments scheme described in Section 9. The following sequence of operations is used to represent the distribution of sensible heat and water vapour through the atmospheric boundary layer.

(i) The fluxes of sensible heat and water vapour F_H and F_W are converted to increments $\delta h'$ and δr which correspond to the changes in h'_{950} and r_{950} that would take place during a time interval $2\delta t$ if all the energy from the surface were retained in that layer. These increments are given by

$$\delta h' = \frac{R}{c_p}\frac{\ln(10/9)}{b} F_H(2\delta t), \qquad \delta r = \frac{g}{b} F_W(2\delta t).$$

The values of $\delta h'$ and δr are at present recalculated after every hour of real time during the integration.

(ii) After each double time-step of integration the increment $\delta h'$ is added to h'_{950}.

(iii) At the same time δr is uniformly distributed among the set of 100-mb layers which form the atmospheric boundary layer, i.e. the set of layers adjacent to the surface which were involved in a convective adjustment at the end of the previous double time-step. If there was no convective adjustment δr is added to r_{950}.

(iv) Finally, the convective adjustments scheme is operated which, if the static stability permits, will redistribute $\delta h'$ through two or more 100-mb layers, whilst leaving the relative humidities of the layers concerned unaltered (see Section 9).

This sequence of operations ensures a rather realistic treatment of the distribution of sensible heat through the atmospheric boundary layer, but the corresponding distribution of water vapour is achieved in a somewhat arbitrary manner.

9. SUB-GRID-SCALE CONVECTION

9.1. *Introduction*

Convective motions with wavelength equal to twice the grid length are known to grow in statically unstable regions of primitive-equation model atmospheres. As well as being a meteorologically unrealistic scale of motion, this so-called grid-scale convection is likely to lead to explosive non-linear computational instabilities. In the real atmosphere, static instability is rapidly neutralized by vertical heat transports associated with small-scale convection (as defined on page 39), and clearly it is important that these transports be represented in the 10-level model so that the development of grid-scale convection may be precluded.

In addition, small-scale convection plays an important role in the general scheme of atmospheric motion by distributing sensible and latent heat from the surface through the lower troposphere (Carlson and Ludlam[35]). Even during periods of 1–2 days this effect may be significant for the development of the large-scale flow if the surface heating is sufficiently intense.

Finally, it is desirable that a representation of small-scale convection be incorporated into the model atmosphere in order that distributions of convective rainfall may be predicted.

9.2. *The convective adjustments scheme*

Small-scale convection grows when the lapse rate of temperature $\gamma(= -\partial T/\partial z)$ exceeds some neutral value γ_c. Vertical heat transports are effected by small-scale convection and these reduce the lapse rate towards its neutral value. Furthermore, these convective transports operate with a very short time-scale so that the static instability is rather rapidly neutralized. Each grid point in the 10-level model represents an area 10^4 km^2. It is reasonable to assume, therefore, that before static instability could develop on the grid scale, γ_c would be exceeded locally within the area represented by a grid point, and small-scale convective transports would then begin. Thus it may be assumed that except in the immediate vicinity of the earth's surface γ_c is never exceeded on the grid scale of the model.

This argument leads to the notion of a convective adjustments scheme as a rather simple method of representing the important effects of small-scale convection in the model atmosphere. After each double time-step of integration the lapse rates in the model atmosphere are everywhere examined, and whenever γ_c has been exceeded as a result of the changes occurring during the time step, convective heat transports are computed which restore γ to its neutral value.

It remains to define γ_c. Manabe *et alii*[36] used a convective adjustment scheme in which the neutral lapse rate was given by

$$\gamma_c = \begin{cases} \gamma_d & \text{for } 0 \leqslant X < 1 \\ \gamma_s & \text{for } X = 1. \end{cases}$$

This scheme has the disadvantage that unrealistically rapid changes in γ may be implied when air achieves large-scale saturation. An experiment in which this scheme was tested in the 10-level model showed that sudden changes can produce serious defects in computed forecasts, and it is believed that this feature has also caused difficulties in other numerical models. The following definition of γ_c has been used in the 10-level model:

$$\gamma_c = \begin{cases} \gamma_d & \text{for } 0 \leqslant X < X_c \\ \gamma_d\left(\dfrac{1-X}{1-X_c}\right) + \gamma_s\left(\dfrac{X-X_c}{1-X_c}\right) & \text{for } X_c \leqslant X \leqslant 1 \end{cases} \quad \ldots (53)$$

where X_c is a threshold relative humidity taken to be 0·5 in the experiments so far conducted; γ_c is now a continuous function of X so that unrealistically sudden changes are avoided. The physical justification for such a definition of γ_c is that saturation may occur locally within a grid square even though $X < 1$. In such a situation convective transports will begin to reduce γ if γ_c is exceeded.

Observations quoted by Roll[21] (p. 300) suggest $X \approx 0{\cdot}75$ as typical of regions of cumulus convection. The corresponding neutral lapse rate given by the above formula is $\gamma_c \approx 0{\cdot}5$ $(\gamma_d + \gamma_s)$, which agrees well with the suggestions of Ludlam.[34]

The vertical transport of water vapour which accompanies convective transport of sensible heat is rather arbitrarily represented by assuming that the relative humidity of each layer involved in a convective adjustment is unchanged by the small-scale convection, except where this would result in an increase of total water content, in which case the relative humidity of the uppermost adjusted layer is reduced. An improved representation of convective water vapour transport would be a great asset for convective adjustment schemes such as this.

Any water in excess of that required to conserve the relative humidities is condensed to form liquid water, and may eventually reach the surface as convective rainfall (see Section 9.4.). The appropriate latent-heat release is taken into account, the finite-difference representation of $\int(c_pT + Lr)\mathrm{d}p$ being conserved in the set of 100-mb layers concerned.

9.3. *Details of the convective adjustment scheme*

After each double time-step of integration in the model the seven levels from 300 mb to 900 mb are tested for instability at every interior h grid-point. (The 200-mb level is reliably stable and is therefore not tested.) The neutral lapse rate γ_c is most conveniently determined at the mid-point of each 100-mb layer, and therefore level k is regarded as unstable if

$$[T]_{k+\frac{1}{2}} - [T]_{k-\frac{1}{2}} > \tfrac{1}{2}[h']_{k+\frac{1}{2}}[\gamma_c]_{k+\frac{1}{2}} + \tfrac{1}{2}[h']_{k-\frac{1}{2}}[\gamma_c]_{k-\frac{1}{2}},$$

where $[T]_{k+\frac{1}{2}}$ and $[T]_{k-\frac{1}{2}}$ are derived from $[h']_{k+\frac{1}{2}}$ and $[h']_{k-\frac{1}{2}}$ using the relationship

$$[T]_{k+\frac{1}{2}} = g[h']_{k+\frac{1}{2}}/R\ln((k+1)/k) \quad \ldots (54)$$

and a similar relationship for $[T]_{k-\frac{1}{2}}$. The square brackets are used here to denote values of variables before convective adjustment. Hence level k is unstable if

$$\left\{\frac{g}{R\ln((k+1)/k)}-\frac{[\gamma_c]_{k+\frac{1}{2}}}{2}\right\}[h']_{k+\frac{1}{2}} > \left\{\frac{g}{R\ln((k/(k-1)}+\frac{[\gamma_c]_{k-\frac{1}{2}}}{2}\right\}[h']_{k-\frac{1}{2}}.$$

The seven levels are tested in this way from the top downwards. If level k_1 is the first found to be unstable, and if k_1+n is the next stable level, the thicknesses and humidity mixing ratios of layers $k_1-\frac{1}{2}$, $k_1+\frac{1}{2}$, ..., $k_1+n-\frac{1}{2}$ are adjusted as follows.

The requirement that levels k_1, k_1+1, ..., k_1+n-1 be neutrally stable after adjustment gives the following n equations in the $n+1$ unknown adjusted thicknesses:

$$\left\{\frac{g}{R\ln((k+1)/k)}-\frac{(\gamma_c)_{k+\frac{1}{2}}}{2}\right\}h'_{k+\frac{1}{2}} = \left\{\frac{g}{R\ln(k/(k-1))}+\frac{(\gamma_c)_{k-\frac{1}{2}}}{2}\right\}h'_{k-\frac{1}{2}}, \qquad \ldots (55)$$

where $k = k_1, k_1+1, \ldots, k_1+n-1$. It is assumed that $(\gamma_c)_{k+\frac{1}{2}} = [\gamma_c]_{k+\frac{1}{2}}$ for $k = k_1, k_1+1, \ldots, k_1+n-1$ since the relative humidities of the layers concerned are, in general, unchanged by the convective adjustments.

The set of simultaneous equations in the adjusted thicknesses is completed by an equation derived from the heat conservation equation

$$\sum_{k=k_1}^{k_1+n}\{c_p([T]_{k-\frac{1}{2}}-T_{k-\frac{1}{2}})+L([r]_{k-\frac{1}{2}}-r_{k-\frac{1}{2}})\} = 0, \qquad \ldots (56)$$

which is valid because each layer of the model atmosphere has the same mass per unit area.

A solution is obtained by assuming that there is net condensation in the layers concerned as a result of the convective adjustments, in which case

$$r_{k-\frac{1}{2}} = [X]_{k-\frac{1}{2}}(r_s)_{k-\frac{1}{2}}, \qquad k = k_1, k_1+1, \ldots, k_1+n.$$

The Clausius-Clapeyron equation gives the following relationship between $(r_s)_{k-\frac{1}{2}}$ and $T_{k-\frac{1}{2}}$,

$$\frac{(r_s)_{k-\frac{1}{2}}-[r_s]_{k-\frac{1}{2}}}{T_{k-\frac{1}{2}}-[T]_{k-\frac{1}{2}}} = \frac{\epsilon L[r_s]_{k-\frac{1}{2}}}{R[T]^2_{k-\frac{1}{2}}}.$$

Thus

$$r_{k-\frac{1}{2}} = [r]_{k-\frac{1}{2}}+\frac{\epsilon L[r]_{k-\frac{1}{2}}}{R[T]^2_{k-\frac{1}{2}}}\{T_{k-\frac{1}{2}}-[T]_{k-\frac{1}{2}}\},$$

and equation (56) becomes

$$\sum_{k=k_1}^{k_1+n}\left[\left\{c_p+\frac{\epsilon L^2[r]_{k-\frac{1}{2}}}{R[T]^2_{k-\frac{1}{2}}}\right\}\left\{T_{k-\frac{1}{2}}-[T]_{k-\frac{1}{2}}\right\}\right] = 0. \qquad \ldots (57)$$

Using equations similar to equation (54) to write equation (57) in terms of thicknesses, and substituting successively from equations (55) into equation (57), a single linear equation in $h'_{k_1-\frac{1}{2}}$ may be obtained. After this equation has been solved equations (55) are used again to obtain the other adjusted thicknesses, and the new values of the saturation mixing ratios are obtained from these thicknesses using the quartic polynomial. The mixing ratio

of liquid water falling through level k_1+n as a result of the convective adjustment is given by

$$M_{k_1+n} = \sum_{k=k_1}^{k_1+n} \{[r]_{k-\frac{1}{2}} - [X]_{k-\frac{1}{2}}(r_s)_{k-\frac{1}{2}}\}.$$

If M_{k_1+n} computed in this way is negative, the assumption that net condensation would occur was false and a second solution is computed with equation (57) replaced by

$$\sum_{k=k_1}^{k_1+n} \{T_{k-\frac{1}{2}} - [T]_{k-\frac{1}{2}}\} = 0.$$

In this case the relative humidity of layer $k_1-\frac{1}{2}$ is reduced in order to conserve total water content, and there is, of course, no net production of liquid water.

A convective adjustment made in this way to layers $k_1-\frac{1}{2}, k_1+\frac{1}{2}, \ldots, k_1+n-\frac{1}{2}$ may possibly create instability at the (previously stable) levels k_1-1 and/or k_1+n. The stability of these levels is therefore tested after such an adjustment and if, for example, level k_1+n has become unstable as a result of the adjustment, the process described above is repeated, this time making adjustments to layers $k_1-\frac{1}{2}, k_1+\frac{1}{2}, \ldots, k_1+n-\frac{1}{2}$ and $k_1+n+\frac{1}{2}$. Thus by an iterative procedure it is ensured that, after the convective adjustments, each column of the model atmosphere is entirely free from static instability according to the criterion described in Section 9.2.

9.4. *The evaporation of convective rainfall*

The rates of convective rainfall predicted in the 10-level model, related to M_{k_1+n} by equation (36), are average values for grid squares with area 10^4 km^2, and consequently are much smaller than local values in the real atmosphere. In order to obtain a more realistic estimate of the effects of evaporation on convective rainfall, the grid-square average rate of convective rainfall P_k is multiplied by a constant before equation (38) is used, and the rate of rainfall P_{k+1} obtained from equation (39) is subsequently divided by the same factor. This factor should be the inverse of the fraction of the grid-square area which is occupied by convective rainfall and, although this is a parameter which varies considerably from case to case, a value of 20 seems to be acceptable.

9.5. *The distribution of small-scale convection in the model atmosphere*

Convective adjustments commonly occur in the model atmosphere in response to heating from the surface, and these have the effect of redistributing sensible heat from the surface through the atmospheric boundary layer (see Section 8.4.).

Outside the atmospheric boundary layer the general structure of the mid-latitude troposphere is determined by the large-scale slope convection and is therefore statically stable and unfavourable for the development of small-scale convection (Carlson and Ludlam[35]). Near fronts, however, two processes may be identified which can effect a destabilization of the atmosphere and thus initiate small-scale convection.

(i) Thermodynamically indirect vertical circulations may be present near fronts (Todsen[37]) and may effect destabilization by differential advection.

(ii) Conditionally unstable air (for which $\gamma_d > \gamma > \gamma_s$) from the boundary layer becomes saturated, and therefore statically unstable, in large-scale frontal ascent (Green *et alii*[38]).

The 10-level model simulates both of these processes so that convective adjustments occur in frontal regions, usually producing convective rainfall which supplements the dynamical rainfall predicted in these regions.

10. AN EXAMPLE OF FORECASTS FROM THE 10-LEVEL MODEL

The most recent date for which forecasts have been produced is 6 February 1969 when initial data at 00 GMT were used. The version of the forecast formulation was that which includes all the effects described in the preceding sections. It is not appropriate to give an extensive account here of the forecasts for this date; the purpose of this section is to show a few of the forecast fields which are obtained from this model. Spatial cross-sections and time cross-sections can easily be extracted from the record on the magnetic tape which contains forecast fields at intervals of one hour, and these cross-sections enable variations in space and time during the forecast period to be studied.

During the 24 hours covered by the forecast a deepening depression moved from a position just north-east of Ocean Weather Station 'I' eastwards towards southern Norway. As the depression moved eastwards a very cold northerly airstream spread across the British Isles giving snow showers, mostly in association with minor troughs in this northerly airstream but also on coasts and slopes exposed to the north winds. Figures 24, 25 and 26

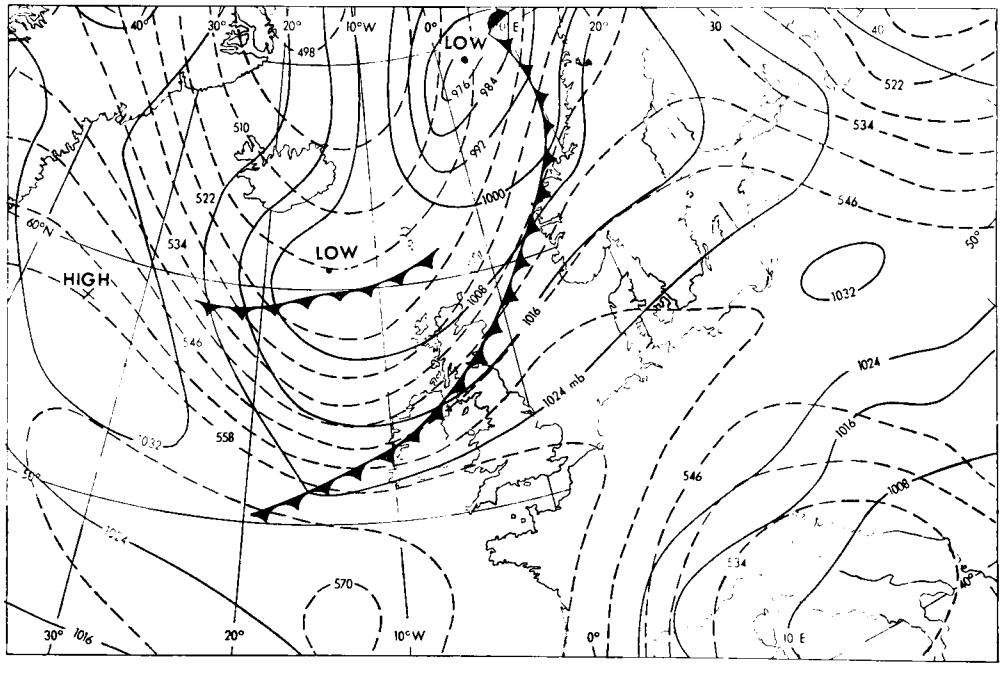

FIGURE 24. Actual synoptic situation at 00 GMT on 6 February 1969 taken from charts of the Central Forecasting Office

—— Surface isobars at intervals of 8 mb
– – – 500-mb contours at intervals of 6 decametres

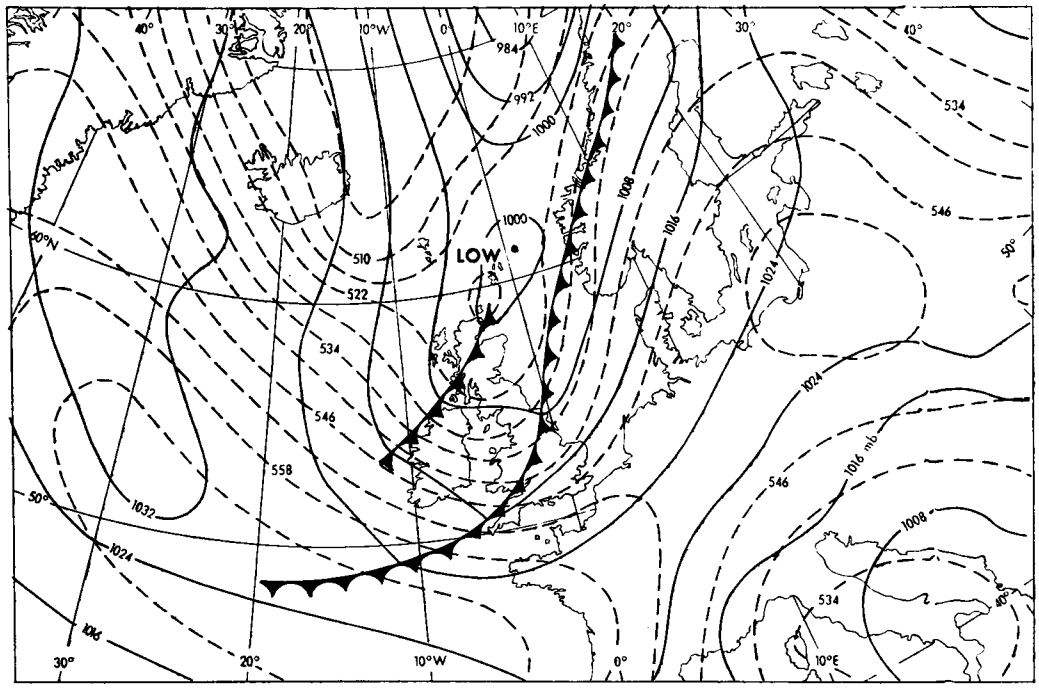

FIGURE 25. Actual synoptic situation at 12 GMT on 6 February 1969 taken from charts of the Central Forecasting Office

—— Surface isobars at intervals of 8 mb - - - 500-mb contours at intervals of 6 decametres

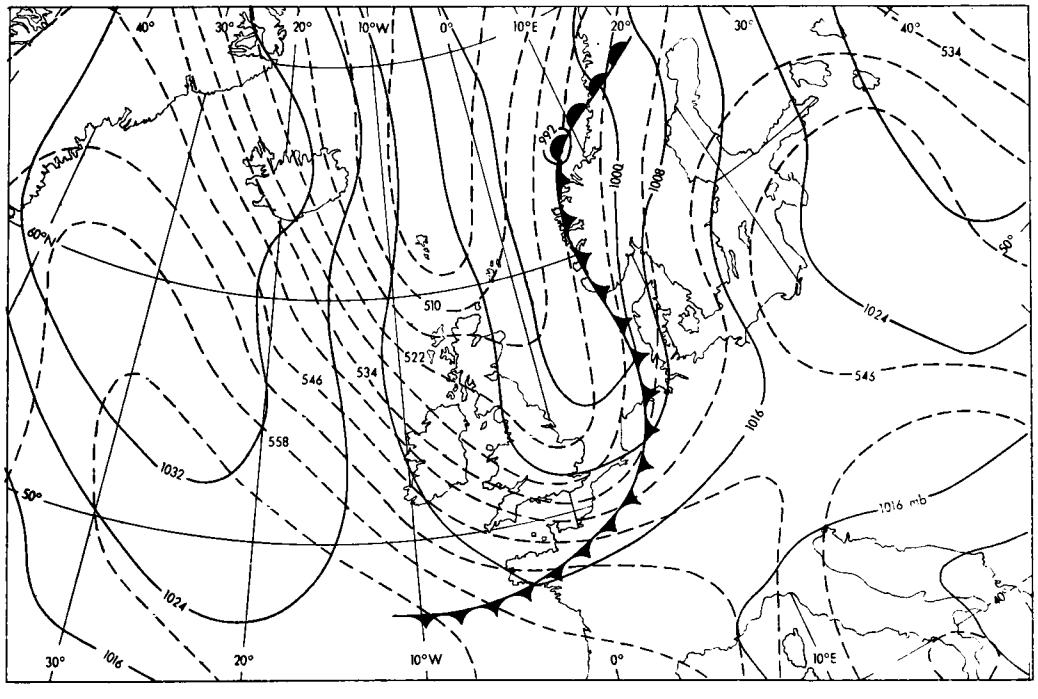

FIGURE 26. Actual synoptic situation at 00 GMT on 7 February 1969 taken from charts of the Central Forecasting Office

—— Surface isobars at intervals of 8 mb - - - 500-mb contours at intervals of 6 decametres

show the surface and 500-mb analyses at 00 GMT and 12 GMT on 6 February and 00 GMT on the 7th, taken from the charts of the Central Forecasting Office, Bracknell. Figures 27 and 28 show the corresponding forecast fields for 12 GMT on the 6th and 00 GMT on the 7th; the development of the depression was not adequately forecast, and the troughs have not been moved sufficiently quickly. Part of the discrepancy may be due to the use of too large a friction coefficient, refinement of which must await the production of a considerable number of 24-hour forecasts.

Figures 29 and 30 show the present weather for the two forecast times mentioned above; these are subjectively drawn from synoptic reports received at the Central Forecasting Office. The areas of steady precipitation have been hatched and heavier hatching has been used to denote areas where the precipitation was reported as moderate. Most of the precipitation was snow and it is difficult to separate the precipitation associated with the troughs from the showery precipitation, though the position of one of these troughs has been indicated on Figure 29, and at a few places this trough gave moderate to heavy snow for a time. The thunderstorm activity has been indicated by the appropriate symbol. Figures 31 and 32 show forecast rates of rain for the same times; the low values of the relevant thicknesses between 1000 mb and the levels 700 mb, 500 mb or 900 mb would have enabled the forecaster to predict snow and not rain. The steady precipitation areas have been hatched, and heavier hatching has been used to indicate an intensity of between 0·5 mm/h and 4 mm/h. The stippled areas delineate those grid points where convective rainfall is expected, as a result of the convective adjustments described in Section 9, the intensity being mostly about 0·01 mm/h. These areas are more extensive than the areas

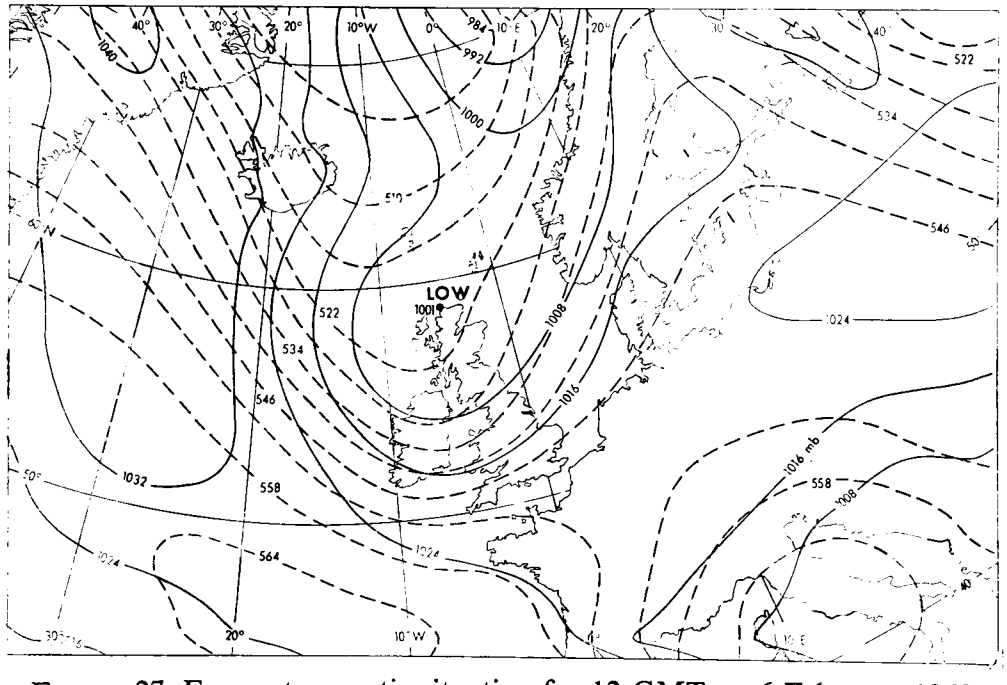

FIGURE 27. Forecast synoptic situation for 12 GMT on 6 February 1969

—— Surface isobars at intervals of 8 mb

– – – 500-mb contours at intervals of 6 decametres

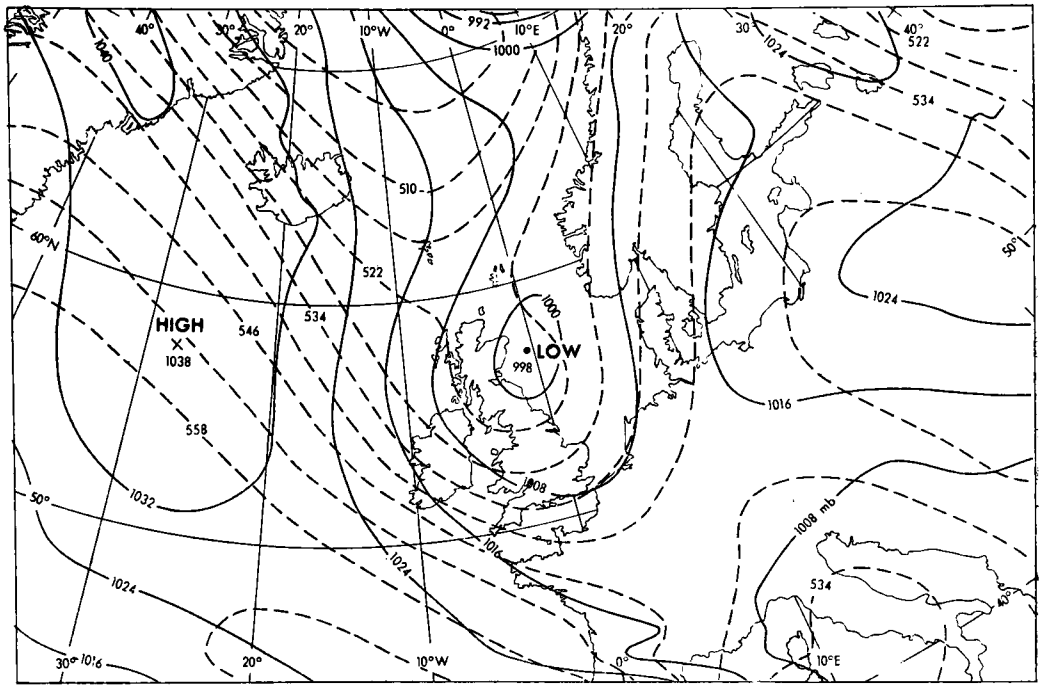

FIGURE 28. Forecast synoptic situation for 00 GMT on 7 February 1969

—— Surface isobars at intervals of 8 mb – – – 500-mb contours at intervals of 6 decametres.

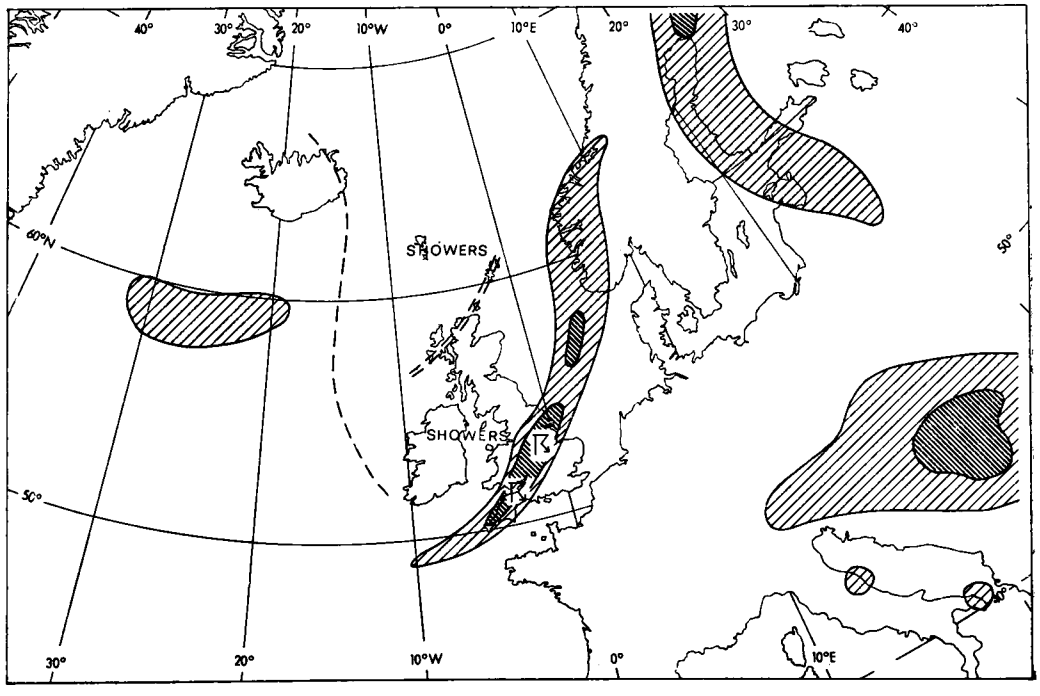

Slight rain, < 0·5 mm/h Moderate rain, 0·5 to 4 mm/h Region of thundery activity

– – – – Estimated boundary of region of widespread showers ==== Trough

FIGURE 29. Present weather at 12 GMT on 6 February 1969

Subjectively drawn from synoptic reports received at Central Forecasting Office.

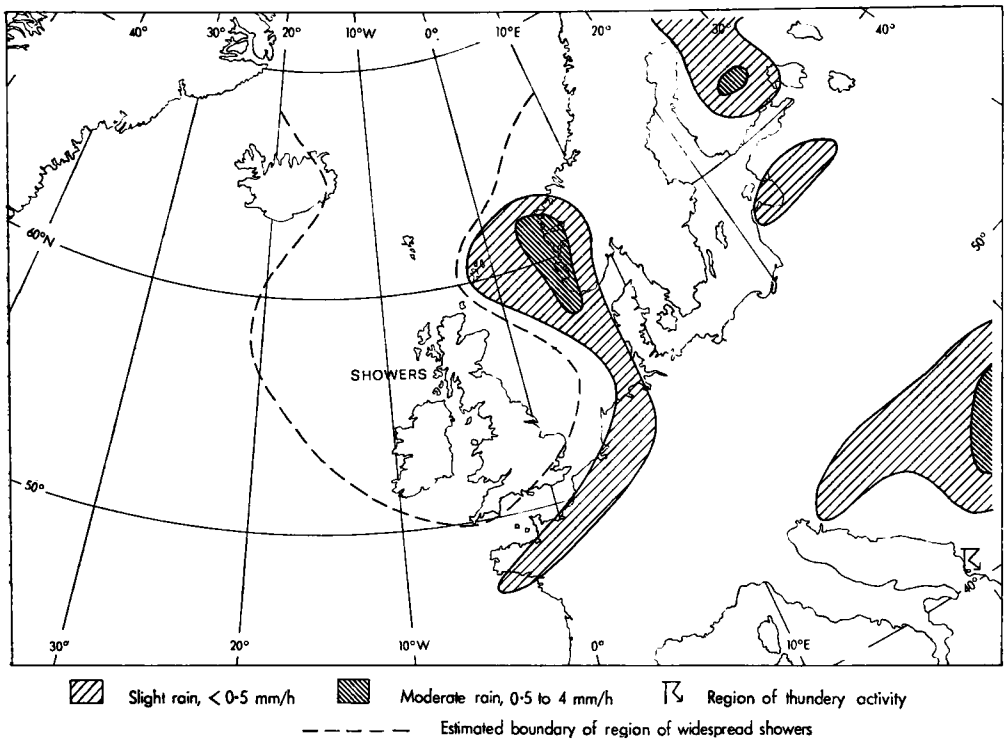

FIGURE 30. Present weather at 00 GMT on 7 February 1969
Subjectively drawn from synoptic reports received at Central Forecasting Office.

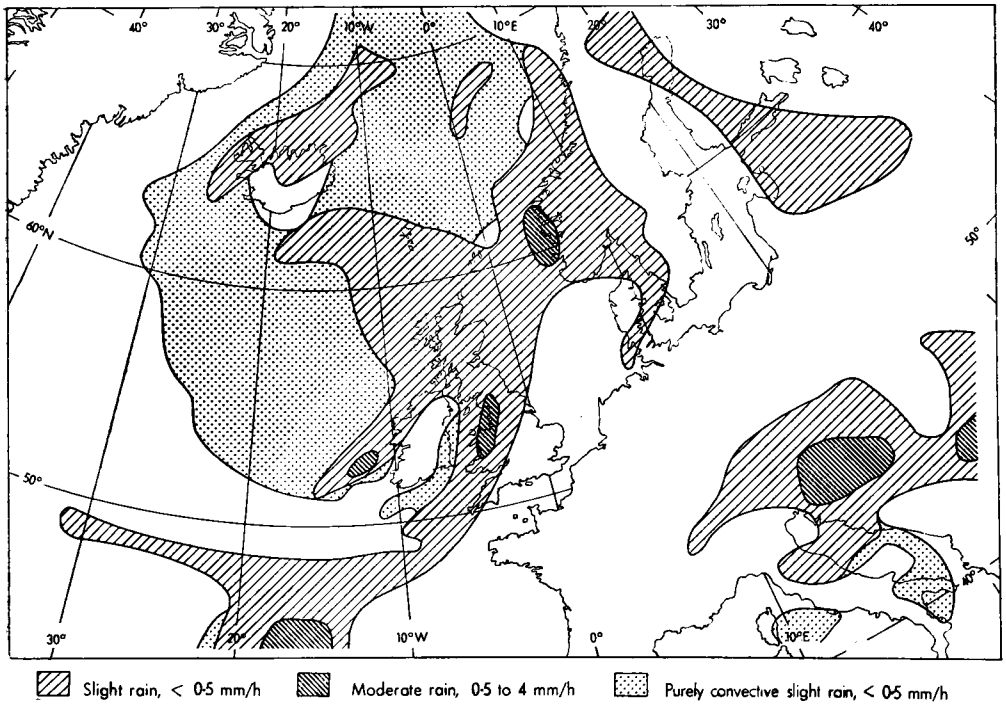

FIGURE 31. Forecast rate of rain for 12 GMT on 6 February 1969

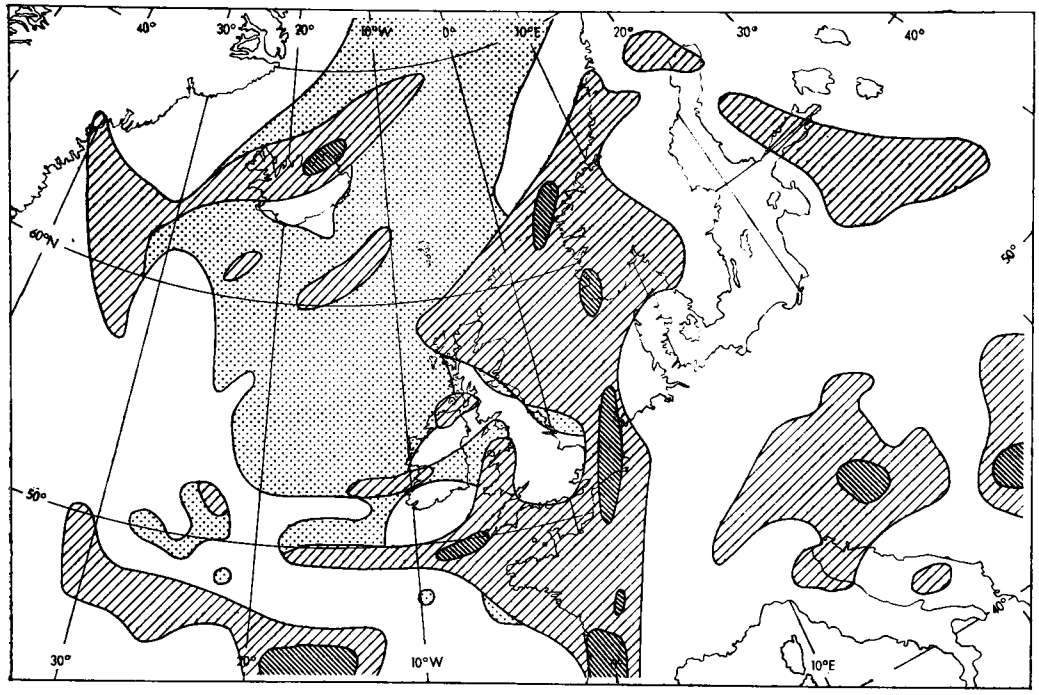

FIGURE 32. Forecast rate of rain for 00 GMT on 7 February 1969

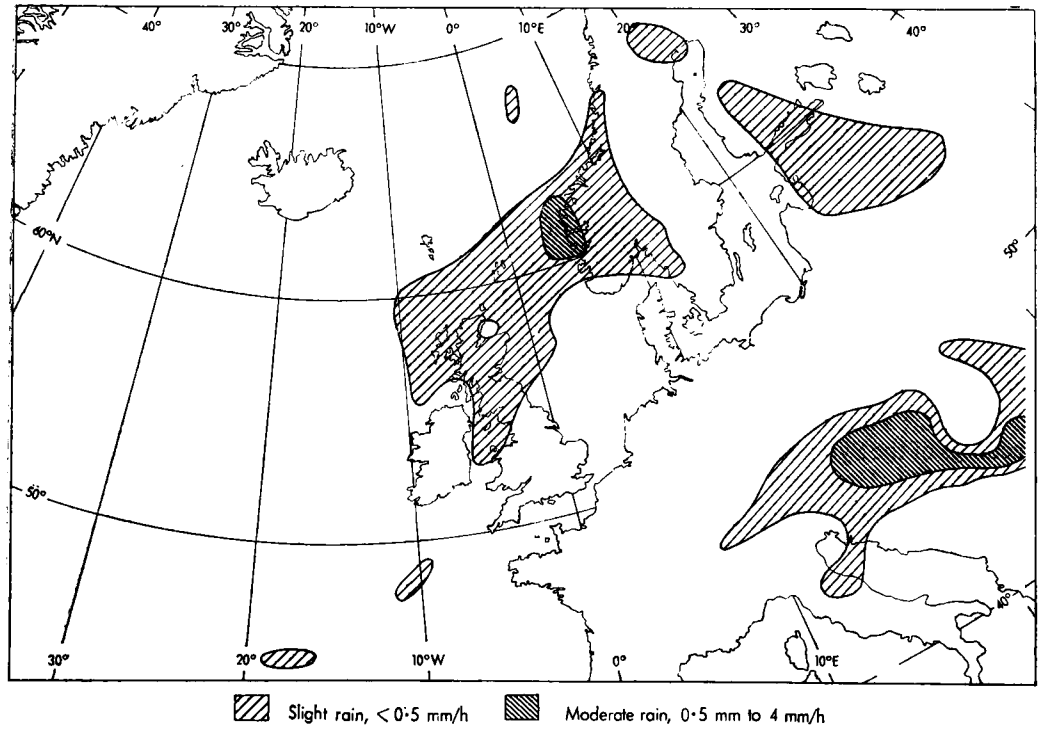

FIGURE 33. Forecast rate of rain for 12 GMT on 6 February with surface heat and moisture fluxes omitted

showing the showery activity on Figures 29 and 30, but as a first approximation there is considerable agreement. Most of this convective rainfall, as well as some of the steady rainfall, arises from the inclusion of the heat and moisture transfers described in Section 8; this is clearer when Figure 31 is compared with Figure 33 which shows the 12-hour forecast obtained from a formulation in which heat and moisture transfers from the surface are omitted; in this figure all the forecast precipitation area has been hatched. These forecasts were obtained from objectively analysed initial data and further comments on them are contained in an article by Atkins.[39]

BIBLIOGRAPHY

1. RICHARDSON, L. F.; Weather prediction by numerical process. Cambridge University Press, 1922.
2. CHARNEY, J. G.; On the scale of atmospheric motions. *Geofys. Publr, Oslo*, **17**, No. 2, 1948.
3. COURANT, R., FRIEDRICHS, K. O. and LEWY, H.; Über die partiellen Differenzen-gleichungen der mathematischen Physik. *Math. Annln, Leipzig*, **100**, 1928, pp. 32–74.
4. BUSHBY, F. H. and TIMPSON, M. S.; A 10-level atmospheric model and frontal rain. *Q. Jnl R. met. Soc., London*, **93**, 1967, pp. 1–17.
5. BENWELL, G. R. R. and BRETHERTON, F. P.; A pressure oscillation in a 10-level atmospheric model. *Q. Jnl R. met. Soc., London*, **94**, 1968, pp. 123–131.
6. ELIASSEN, A.; A procedure for numerical integration of the primitive equations of the two-parameter model of the atmosphere. Los Angeles, Univ. Calif., Dep. Met., 1956 (Contract AF 19(604)-1286, Large-scale synoptic processes.).
7. PHILLIPS, N. A.; Numerical integration of the hydrostatic system of equations with a modified version of the Eliassen finite-difference grid. SIGEKATA SYONO (editor); Proceedings of the International Symposium on Numerical Weather Prediction in Tokyo, November 7–13, 1960. Tokyo, Meteorological Society of Japan, 1962, pp. 109–119.
8. BENWELL, G. R. R. and TIMPSON, M. S.; Further work with the Bushby-Timpson 10-level model. *Q. Jnl R. met. Soc., London*, **94**, 1968, pp. 12–24.
9. WALLINGTON, C. E.; The use of smoothing or filtering operators in numerical forecasting. *Q. Jnl R. met. Soc., London*, **88**, 1961, pp. 470–484.
10. THOMPSON, P. D.; Numerical weather analysis and prediction. New York, Macmillan, 1961.
11. KRISHNAMURTI, T. N.; Diagnostic studies of weather systems of low and high latitudes (Rossby Number < 1). Los Angeles, Univ. Calif., Dep. Met., 1967 (Contract AF 19(628)-4777 Final Report).
12. SHUMAN, F. G.; Numerical methods in weather prediction: II. Smoothing and filtering. *Mon. Weath. Rev. U.S. Dep. Agric., Washington*, **85**, 1957, pp. 357–361.
13. SAWYER, J. S.; The introduction of the effects of topography into methods of numerical forecasting. *Q. Jnl R. met. Soc., London*, **88**, 1959, pp. 31–43.
14. DEACON, E. L.; The drag of the wind on the sea. Hamburg, Institut für Meereskunde der Universität. Proceedings of the Symposium on Mathematical-Hydrodynamical Methods of Physical Oceanography, September 1961. Hamburg 1962.
15. FINDLATER, J., HARROWER, T. N. S., HOWKINS, G. A. and WRIGHT, H. L.; Surface and 900 mb wind relationships. *Scient. Pap., met. Off., London*, No. 23, 1966.
16. CRESSMAN, G. P.; Improved terrain effects in barotropic forecasts. *Mon. Weath, Rev. U.S. Dep. Agric., Washington*, **88**, 1960, pp. 327–342.
17. PASQUILL, F.; Atmospheric diffusion. London, D. Van Nostrand, 1962.
18. SUTCLIFFE, R. S.; Surface resistance in atmospheric flow. *Q. Jnl R. met. Soc., London*, **62**, 1936, pp. 3–12.
19. BEST, A. C.; The evaporation of raindrops. *Q. Jnl R. met. Soc., London*. **78**, 1952, pp. 200–225.

20. BEST, A. C.; The size distribution of raindrops. *Q. Jnl R. met. Soc., London*, **76**, 1950, pp. 16–36.

21. ROLL, H. U.; Physics of the marine atmosphere. International Geophysics Series Vol. 7. New York and London, Academic Press, 1965.

22. CRAIG, R. A.; Measurements of temperature and humidity in the lowest 1000 feet of the atmosphere over Massachusetts Bay. *Pap. phys. Oceanogr. Met., Cambridge, Mass.*, **10**, No. 1, 1946.

23. ROBINSON, G. D.; Another look at some problems of the air–sea interface. *Q. Jnl R. met. Soc., London*, **92**, 1966, pp. 451–465.

24. MANABE, S.; On the modification of air-mass over the Japan Sea when the outburst of cold air predominates. *Jnl met. Soc. Japan, Tokyo*, Second Series, **35**, 1957, pp. 311–326.

25. PENMAN, H. L.; Natural evaporation from open water, bare soil, and grass. *Proc. R. Soc., London*, A, **193**, 1948, pp. 120–145.

26. MONTEITH, J. L. and SZEICZ, G.; Radiative temperature in the heat balance of natural surfaces. *Q. Jnl R. met. Soc., London*, **88**, 1962, pp. 496–507.

27. LUMB, F. E.; The influence of cloud on hourly amounts of total solar radiation at the sea surface. *Q. Jnl R. met. Soc., London*, **90**, 1964, pp. 43–56.

28. SMAGORINSKY, J.; On the dynamical prediction of large-scale condensation by numerical methods. *Geophys. Monogr., Washington*, No. 5, 1960, pp. 71–78.

29. ROBINSON, G. D.; Some observations from aircraft of surface albedo and the albedo and absorption of cloud. *Arch. Met. Geophys. Bioklim., Wien.*, **9**, 1958, pp. 28–41.

30. MONTEITH, J. L.; Attenuation of solar radiation: a climatological study. *Q. Jnl R. met. Soc., London*, **88**, 1962, pp. 508–521.

31. KONDRAT'YEV, K.Ya.; Radiative heat exchange in the atmosphere. Oxford, Pergamon Press, 1965 (translated from the Russian, first published 1956).

32. BROOKS, F. A. and GODDARD, W. B.; Observed four-component hourly energy balances. BROOKS, F. A. *et alii*; Investigation of energy, momentum and mass transfers near the ground. Davis, Univ. Calif., Dep. Agric. Engrg and Dep. Wat. Sci. Engrg, 1966 (Grant DA-AMC-28-043-65-512, Final Report), pp. 5–24.

33. SZEICZ, G., ENDRODI, G. and TAJCHMAN, S.; Aerodynamic and surface factors in evaporation. *Wat. Resour. Res., Washington*, **5**, 1969, pp. 380–394.

34. LUDLAM, F. H.; Cumulus and cumulonimbus convection. *Tellus, Stockholm*, **18**, 1966, pp. 687–698.

35. CARLSON, T. N. and LUDLAM, F. H.; Large-scale conditions for the occurrence of severe local storms. Part I *of* Research on characteristics of severe storms. London, Imperial College Sci. Tech., Dep. Met. (Grant AF EOAR 64–60).

36. MANABE, S., SMAGORINSKY, J. and STRICKLER, R. F.; Simulated climatology of a general circulation model with a hydrologic cycle. *Mon. Weath. Rev. U.S. Dep. Agric., Washington*, **93**, 1965, pp. 769–798.

37. TODSEN, M.; A computation of the vertical circulation in a frontal zone from the quasi-geostrophic equations. *Oslo Univ., Inst. Theor. Met., Tech. Note* No. 4, 1964.

38. GREEN, J. S. A., LUDLAM, F. H. and MCILVEEN, J. F. R.; Isentropic relative-flow analysis and the parcel theory. *Q. Jnl R. met. Soc., London*, **92**, 1966, pp. 210–219.

39. ATKINS, M. J.; Objective analysis of upper air height and humidity data on a fine mesh. *Met. Mag., London*, **99**, 1970, pp. 98–110.

APPENDIX I. EXAMPLES OF ALGORITHMS USED IN FINITE-DIFFERENCE SCHEME

We will assume $x = 0$, $y = 0$ at the bottom left-hand corner of the grid shown in Figure 1, page 4. The notation $Z(i, j, k, t)$ will refer to the value at time t of variable Z at the grid point $x = ia$, $y = ja$, $p = kb$. i, j and k are integers such that $0 \leqslant i \leqslant 94$, $0 \leqslant j \leqslant 62$ and $1 \leqslant k \leqslant 10$. The notation $\Sigma Z(i, j, k, t)$ is defined as equivalent to $Z(i+1, j+1, k, t)+Z(i-1, j+1, k, t)+Z(i+1, j-1, k, t)+Z(i-1, j-1, k, t)$.

Two examples of the algorithms are shown in this appendix. The first gives u at time $t+\delta t$ in terms of variables at time t, and the second gives u at time $t+2\delta t$ in terms of variables at time t and at time $t+\delta t$.

Example A

u (at time $t+\delta t$) is only evaluated for i odd, j even.

For $2 \leqslant k \leqslant 9$, $2 \leqslant j \leqslant 60$

$$u(i, j, k, t+\delta t) = \tfrac{1}{4}\,\Sigma u(i, j, k, t)+\delta t\Big[\frac{g}{2b}\{\tau_x(i, j, k+1, t)-\tau_x(i, j, k-1, t)\}+$$

$$+f(i, j)v(i, j, k, t)-\frac{m(i, j)}{16a}[\Sigma u(i, j, k, t)\{u(i+1, j+1, k, t)-$$

$$-u(i-1, j+1, k, t)+u(i+1, j-1, k, t)-u(i-1, j-1, k, t)\}+$$

$$+4v(i, j, k, t)\{u(i+1, j+1, k, t)-u(i+1, j-1, k, t)+u(\mathrm{i}-1, \mathrm{j}+1, k, t,)-$$

$$-u(i-1, j-1, k, t)\}+8g\{h(i+1, j, k, t)-h(i-1, j, k, t)\}]-\frac{1}{16b}\{\omega(i, j+1, k, t)+$$

$$+\omega(i, j-1, k, t)\}\{\Sigma u(i, j, k+1, t)-\Sigma u(i, j, k-1, t)\}\Big].$$

For $k = 1$, $2 \leqslant j \leqslant 60$

The last term in curly brackets is replaced by

$$2\{\Sigma u(i, j, 2, t)-\Sigma u(i, j, 1, t)\},$$

and the first term in curly brackets is zero.

For $k = 10$, $2 \leqslant j \leqslant 60$

The last term in curly brackets is replaced by

$$2\{\Sigma u(i, j, 10, t)-\Sigma u(i, j, 9, t)\},$$

and the first term in curly brackets by

$$2\{\tau_x(i, j, 10, t)-\tau_x(i, j, 9, t)\}.$$

For $2 \leqslant k \leqslant 9$, $j = 0$

$$u(i, j, k, t+\delta t) = \tfrac{1}{2}\{u(i+1, j+1, k, t)+u(i-1, j+1, k, t)\}+$$

$$+\delta t\Big[\frac{g}{2b}\{\tau_x(i, j, k+1, t)-\tau_x(i, j, k-1, t)\}+f(i, j)v(i, j, k, t)-$$

$$-\frac{m(i, j)}{4a}[\{u(i+1, j+1, k, t)+u(i-1, j+1, k, t)\}\{u(i+1, j+1, k, t)-$$

$$-u(i-1, j+1, k, t)\}+2g\{h(i+1, j, k, t)-h(i-1, j, k, t)\}]-$$

$$-\frac{1}{4b}\omega(i, j+1, k, t)\{u(i+1, j+1, k+1, t)+u(i-1, j+1, k+1, t)-$$

$$-u(i+1, j+1, k-1, t)-u(i-1, j+1, k-1, t)\}\Big].$$

For $k = 1, j = 0$

The first term in curly brackets is zero and the last term in curly brackets is replaced by

$$2\{u(i+1, j+1, 2, t) + u(i-1, j+1, 2, t) - u(i+1, j+1, 1, t) - u(i-1, j+1, 1, t)\}.$$

For $k = 10, j = 0$

The last term in curly brackets is replaced by

$$2\{u(i+1, j+1, 10, t) + u(i-1, j+1, 10, t) - u(i-1, j+1, 9, t) - u(i+1, j+1, 9, t)\},$$

and the first term in curly brackets by

$$2\{\tau_x(i, j, 10, t) - \tau_x(i, j, 9, t)\}.$$

For $1 \leqslant k \leqslant 10, j = 62$

The algorithms for $j = 0$ hold except that index $j+1$ must be replaced by $j-1$.

Example B

u(at time $t+2\delta t$) is only evaluated for i even, j odd.

For $2 \leqslant k \leqslant 9, 2 \leqslant i \leqslant 92, 3 \leqslant j \leqslant 61$

$$\begin{aligned} u(i, j, k, t+2\delta t) = {} & u(i, j, k, t) + 2\delta t\Big[\frac{g}{2b}\{\tau_x(i, j, k+1, t+\delta t) - \tau_x(i, j, k-1, t+\delta t)\} + \frac{K(i, j)}{a^2} \times \\ & \times \{u(i+2, j, k, t) + u(i-2, j, k, t) + u(i, j+2, k, t) + u(i, j-2, k, t) - 4u(i, j, k, t)\} + \\ & + f(i, j)v(i, j, k, t+\delta t) - \frac{m(i, j)}{16a}[\Sigma u(i, j, k, t+\delta t)\{u(i+1, j+1, k, t+\delta t) - \\ & - u(i-1, j+1, k, t+\delta t) + u(i+1, j-1, k, t+\delta t) - u(i-1, j-1, k, t+\delta t)\} + \\ & + 4v(i, j, k, t+\delta t)\{u(i+1, j+1, k, t+\delta t) - u(i+1, j-1, k, t+\delta t) + \\ & + u(i-1, j+1, k, t+\delta t) - u(i-1, j-1, k, t+\delta t)\} + 8g\{h(i+1, j, k, t+\delta t) - \\ & - h(i-1, j, k, t+\delta t)\}] - \frac{1}{16b}\{\omega(i, j+1, k, t+\delta t) + \omega(i, j-1, k, t+\delta t)\} \times \\ & \times \{\Sigma u(i, j, k+1, t+\delta t) - \Sigma u(i, j, k-1, t+\delta t)\}\Big]. \end{aligned}$$

For $k = 1, 2 \leqslant i \leqslant 92, 3 \leqslant j \leqslant 61$

The last term in curly brackets is replaced by

$$2\{\Sigma u(i, j, 2, t+\delta t) - \Sigma u(i, j, 1, t+\delta t)\},$$

and the first term in curly brackets is zero.

For $k = 10, 2 \leqslant i \leqslant 92, 3 \leqslant j \leqslant 61$

The last term in curly brackets is replaced by

$$2\{\Sigma u(i, j, 10, t+\delta t) - \Sigma u(i, j, 9, t+\delta t)\},$$

and the first term in curly brackets by

$$2\{\tau_x(i, j, 10, t+\delta t) - \tau_x(i, j, 9, t+\delta t)\}.$$

For $i = 0, i = 94$

$$u(i, j, k, t+2\delta t) = u(i, j, k, t).$$

For $2 \leqslant k \leqslant 9$, $2 \leqslant i \leqslant 92$, $j = 1$

$$u(i,j,k,t+2\delta t) = u(i,j,k,t) + 2\delta t\Big[\frac{g}{2b}\{\tau_x(i,j,k+1,t+\delta t) - \tau_x(i,j,k-1,t+\delta t)\} + \frac{K(i,j)}{a^2} \times$$
$$\times \{u(i+2,j,k,t) + u(i-2,j,k,t) + u(i,j+2,k,t) - 3u(i,j,k,t)\} +$$
$$+ f(i,j)v(i,j,k,t+\delta t) - \frac{m(i,j)}{16a}[\Sigma u(i,j,k,t+\delta t)\{u(i+1,j+1,k,t+\delta t) -$$
$$- u(i-1,j+1,k,t+\delta t) + u(i+1,j-1,k,t+\delta t) - u(i-1,j-1,k,t+\delta t)\} +$$
$$+ 4v(i,j,k,t+\delta t)\{u(i+1,j+1,k,t+\delta t) - u(i+1,j-1,k,t+\delta t) +$$
$$+ u(i-1,j+1,k,t+\delta t) - u(i-1,j-1,k,t+\delta t)\} + 8g\{h(i+1,j,k,t+\delta t) -$$
$$- h(i-1,j,k,t+\delta t)\}] - \frac{1}{8b}\omega(i,j+1,k,t+\delta t)\{\Sigma u(i,j,k+1,t+\delta t) -$$
$$- \Sigma u(i,j,k-1,t+\delta t)\}\Big].$$

For $k = 1$, $j = 1$, $2 \leqslant i \leqslant 92$

The first term in curly brackets is zero and the last term in curly brackets is replaced by

$$2\{\Sigma u(i,j,2,t+\delta t) - \Sigma u(i,j,1,t+\delta t)\}.$$

For $k = 10$, $j = 1$, $2 \leqslant i \leqslant 92$

The last term in curly brackets is replaced by

$$2\{\Sigma u(i,j,10,t+\delta t) - \Sigma u(i,j,9,t+\delta t)\},$$

and the first term in curly brackets by

$$2\{\tau_x(i,j,10,t+\delta t) - \tau_x(i,j,9,t+\delta t)\}.$$

For $1 \leqslant k \leqslant 10$, $2 \leqslant i \leqslant 92$, j = 63

The algorithms are similar to those for $j = 1$ except that the index $j+2$ must be replaced by the index $j-2$, and the index $j+1$ in the ω term must be replaced by the index $j-1$.

APPENDIX II. CRITERION FOR COMPUTATIONAL STABILITY IN 10-LEVEL MODEL

by M. A. L. FARR, B.Sc. and R. P. W. LEWIS, M.A., M.Sc.

Neglecting humidity, the basic variables of the 10-level model are u, v, and h at each of 10 pressure levels. Difficulties arise if we attempt to consider several levels in the vertical, so for our present purpose we shall study the following much simpler set of equations

$$\frac{\partial u}{\partial t} = -u\frac{\partial u}{\partial x} - v\frac{\partial u}{\partial y} - g\frac{\partial h}{\partial x} + fv$$

$$\frac{\partial v}{\partial t} = -u\frac{\partial v}{\partial x} - v\frac{\partial v}{\partial y} - g\frac{\partial h}{\partial y} - fu$$

$$\frac{\partial h}{\partial t} = -u\frac{\partial h}{\partial x} - v\frac{\partial h}{\partial y} - \omega\frac{\partial h}{\partial p} \qquad \text{at 1000 mb}$$

and

$$\omega = -p_{1000}\left(\frac{\partial u}{\partial x} + \frac{\partial v}{\partial y}\right).$$

If we regard u and v as being an average over the model's 10 levels, then ω will have the same value as dp/dt at 1000 mb in the model. The above set of equations will reproduce the same external gravity waves as the 10-level model.

Suppose u_0, v_0, H are solutions, steady in time, and with small spatial variation; then, if we consider a small superposed perturbation u', v', $\phi' = gh'$, neglect of 2nd-order terms gives the following equations which are *linear*:

$$\left.\begin{aligned}
\frac{\partial u'}{\partial t} &= -\frac{\partial \phi'}{\partial x} - u_0\frac{\partial u'}{\partial x} - v_0\frac{\partial u'}{\partial y} + fv' \\
\frac{\partial v'}{\partial t} &= -\frac{\partial \phi'}{\partial y} - u_0\frac{\partial v'}{\partial x} - v_0\frac{\partial v'}{\partial y} - fu' \\
\frac{\partial \phi'}{\partial t} &= -\Phi\left(\frac{\partial u'}{\partial x} + \frac{\partial v'}{\partial y}\right) - u_0\frac{\partial \phi'}{\partial x} - v_0\frac{\partial \phi'}{\partial y}
\end{aligned}\right\}. \qquad \ldots (1)$$

[We have used $\left(\frac{\partial h}{\partial p}\right)_{1000} = -\frac{1}{g\rho_{1000}}$ and put $\Phi = \left(\frac{p}{\rho}\right)_{1000}$.]

Equations (1) correspond to N. A. Phillips's equations (3)–(5).[7] Following Phillips, we assume a wave solution; so, at the (p, q)th grid-point at time step n, we have

$$u'_{pqn} = U_n\Phi^{\frac{1}{2}} \exp i(\alpha p + \beta q),$$

$$v'_{pqn} = V_n\Phi^{\frac{1}{2}} \exp i(\alpha + \beta) \exp i(\alpha p + \beta q),$$

$$\phi'_{p,n} = H_n\Phi \exp i\beta \exp i(\alpha p + \beta q).$$

If the wavelength in the x direction is L_x, then $\alpha = 2\pi a/L_x$; similarly $\beta = 2\pi a/L_y$. Note that in Phillips's paper, the spatial increment is given by $\Delta x = \Delta y = 2a$, and the time increment by $\Delta t = 2\delta t$. The shortest wavelength that can be represented by the grid is $2\Delta x = 4a$, corresponding to $\alpha = \pi/2$; our α and β are equal to *half* the angles defined by Phillips.

In the 10-level model, variables at the odd time-step, i.e. u, $\hat{v}$, and $\hat{\phi}$, are forecast by a forward time-step and spatial derivatives are represented by simple centred differences (see Figure 34). The value at an even time-step of a variable required at the centre of the square formed by the four points at which it is kept is the average of its values at these four points.

Using the formulae

$$\tfrac{1}{2}(e^{i\theta} + e^{-i\theta}) = \cos\theta, \text{ and } \tfrac{1}{2}(e^{i\theta} - e^{-i\theta}) = i\sin\theta,$$

the even to odd time-step is represented by the matrix equation

$$Z_{n+1} = Z_n \cos\alpha\cos\beta - iGZ_n, \qquad \ldots (2)$$

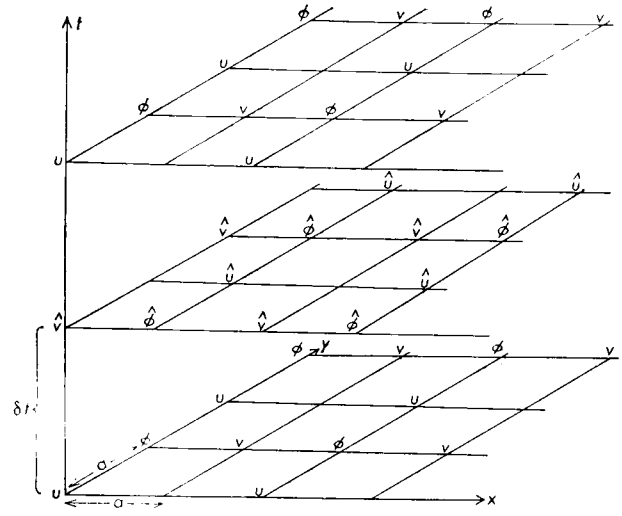

FIGURE 34. x, y, t diagram showing the location of grid-point values of u, v, ϕ
a = horizontal grid length.

where Z_n is the vector

$$\begin{bmatrix} U_n \\ V_n \\ H_n \end{bmatrix}$$

and G is the matrix

$$\begin{bmatrix} \lambda(u_0 \sin\alpha\cos\beta + v_0\cos\alpha\sin\beta) & if\delta t & \lambda\Phi^{\frac{1}{2}}\sin\alpha \\ -if\delta t & \lambda(u_0\sin\alpha\cos\beta + v_0\cos\alpha\sin\beta) & \lambda\Phi^{\frac{1}{2}}\sin\beta \\ \lambda\Phi^{\frac{1}{2}}\sin\alpha & \lambda\Phi^{\frac{1}{2}}\sin\beta & \lambda(u_0\sin\alpha\cos\beta + v_0\cos\alpha\sin\beta) \end{bmatrix}$$

where $\lambda \equiv \delta t/a$.

Values at even time-steps are forecast by a centred time-step, and this is represented by the matrix equation

$$Z_{n+2} = Z_n - 2i\,GZ_{n+1}. \qquad \ldots (3)$$

If we write $\eta = \cos\alpha\cos\beta$ then

$$Z_{n+2} = [I - 2G(i\eta I + G)]Z_n \equiv HZ_n, \qquad \ldots (4)$$

where I is the unit matrix. G is Hermitian and therefore has orthogonal eigenvectors. The eigenvectors of G are also eigenvectors of H, so a necessary and sufficient condition for computational stability is that $\lim_{\delta t \to 0} |\mu_i| \leqslant 1$ for each eigenvalue μ_i of H.

If we write

$$G \equiv \begin{bmatrix} W & iF & M \\ -iF & W & N \\ M & N & W \end{bmatrix}$$

then the eigenvalues of G are

$$C_1 = W;\ C_2 = W + \sqrt{(F^2+M^2+N^2)};\ C_3 = W - \sqrt{(F^2+M^2+N^2)}. \qquad \ldots (5)$$

Using the relationship between G and H, we obtain

$$\mu_i = 1-2C_i^2-2i\eta C_i;$$

therefore

$$|\mu_i|^2 = 1-4C_i^2+4C_i^4+4\eta^2C_i^2 \qquad \ldots (6)$$

and the stability criterion becomes

$$\lim_{\delta t \to 0} (C_i^2+\eta^2) \leqslant 1.$$

Since $F \to 0$ as $\delta t \to 0$, this term may be neglected (see Phillips[7]), leaving the three conditions

$$\left.\begin{aligned} &W^2+\eta^2 \leqslant 1\\ &\{W+\sqrt{(M^2+N^2)}\}^2+\eta^2 \leqslant 1\\ &\{W-\sqrt{(M^2+N^2)}\}^2+\eta^2 \leqslant 1 \end{aligned}\right\} \quad \text{assuming } \lambda = \frac{\delta t}{a} \text{ remains constant as } \delta t \to 0,$$

which can be replaced by

$$\{|W|+\sqrt{(M^2+N^2)}\}^2 \leqslant 1-\eta^2,$$

i.e.

$$\lambda^2\{u_0 \sin\alpha\cos\beta+v_0\cos\alpha\sin\beta)+\Phi^{\frac{1}{2}}(\sin^2\alpha+\sin^2\beta)^{\frac{1}{2}}\}^2 \leqslant 1-\cos^2\alpha\cos^2\beta. \qquad \ldots (7)$$

This is a condition for λ, and must hold for all possible values of u_0, v_0, α, β, and Φ.

Put $\Phi^{\frac{1}{2}} = c$, and define R and θ by $c\,R\cos\theta = u_0$; $c\,R\sin\theta = v_0$; then

$$\lambda^2 \leqslant S^2 \equiv \frac{1-\cos^2\alpha\cos^2\beta}{c^2\{R(\cos\theta\sin\alpha\cos\beta+\sin\theta\cos\alpha\sin\beta)+\sqrt{(\sin^2\alpha+\sin^2\beta)}\}^2}. \qquad \ldots (8)$$

Minimizing S^2 with respect to θ gives $\tan\theta = \cot\alpha\tan\beta$, and inserting this value gives

$$S^2 = \frac{1-\cos^2\alpha\cos^2\beta}{c^2\{R\sqrt{(\cos^2\alpha\sin^2\beta+\sin^2\alpha\cos^2\beta)}+\sqrt{(\sin^2\alpha+\sin^2\beta)}\}^2}.$$

We now make the substitutions

$$x = \cos^2\alpha+\cos^2\beta,\ y = \cos^2\alpha\cos^2\beta,$$

giving

$$S^2 = \frac{1-y}{c^2\{R\sqrt{(x-2y)}+\sqrt{(2-x)}\}^2}. \qquad \ldots (9)$$

Minimizing S^2 with respect to x, we find that the minimum occurs where

$$x = \frac{2(R^2+y)}{R^2+1}, \qquad \ldots (10)$$

and if we substitute this value of x, all the y factors cancel giving

$$S^2 = \frac{1}{2c^2(1+R^2)}.$$

In view of restrictions which should have been placed upon x and y this minimum may be too small, though for most values of R it will be correct. Certainly

$$\delta t \leqslant \frac{a}{\sqrt{(2c^2(1+R^2))}} \qquad \ldots (11)$$

will be a sufficient condition for computational stability.

Typical values for the extremes of c and R used in the model are

$$c^2 = \frac{1000}{\rho_{1000}} = \frac{g\times 1000}{g\rho_{1000}} = \frac{9{\cdot}8\times 1000\times h'_{950}}{100} = 9{\cdot}8\times 10\times 940$$

($h'_{950} = 940$ m corresponds to a temperature of 31°C); therefore $c \approx 304$ m/s.

If we allow for winds of up to 100 m/s then $R = \frac{1}{3}$ and $\delta t \leqslant a/452$ s; for winds up to 150 m/s, $R = \frac{1}{2}$ and $\delta t \leqslant a/480$ s. At 35°N, $a \approx 42\,850$ m. Hence, for winds up to 100 m/s, $\delta t \leqslant 94$ s; for winds up to 150 m/s, $\delta t \leqslant 89$ s.

The effect upon the stability criterion of the inclusion of horizontal diffusion terms for h, u, and v

At present in the 10-level model, the effect of horizontal diffusion is represented by a forward difference from even to even time-step; for example

$$U_{n+2} = U_n + 2\delta t\left(\frac{\partial u}{\partial t}\right)_{n+1} + 2\delta t \,.\, K\nabla^2 U_n.$$

No diffusion is incorporated in the even to odd step. The effect of the diffusion term is to add the expression

$$-\frac{2K\delta t}{a^2}(\sin^2\alpha + \sin^2\beta) \equiv -D$$

to the diagonal elements of the matrix H defined on page 56. If the eigenvalues of this matrix, as modified. are called μ'_i, then the criterion for stability becomes

$$|\mu'_i|^2 = 4C_i^4 - 4C_i^2(1-\eta^2-D) + (1-D)^2 \leqslant 1, \qquad \ldots (12)$$

where C_i are the eigenvalues of G as before. If we write $C_i = \lambda C'_i$, then we have

$$\{(\lambda C'_i)^2 - \tfrac{1}{2}(1-\eta^2-D)\}^2 \leqslant \tfrac{1}{4}(1-\eta^2-D)^2 + \frac{D}{4}(2-D),$$

or

$$\lambda^2 \leqslant \frac{1}{(C'_i)^2}[\tfrac{1}{2}(1-\eta^2-D) + \tfrac{1}{2}\{(1-\eta^2-D)^2 + D(2-D)\}^{\frac{1}{2}}], \qquad \ldots (13)$$

for all θ, α, β, c, and R. The only part of the right-hand side of the last inequality that depends on θ is the factor $1/(C'_i)^2$, so that for stability we want the value of θ that maximizes $(C'_i)^2$. Hence the previous analysis for θ applies equally well now, giving $\tan\theta = \cot\alpha \tan\beta$ as before. This gives as eigenvalues for G:

$$C_1 = W; \quad C_2 = W + \sqrt{(M^2+N^2)}; \quad C_3 = W - \sqrt{(M^2+N^2)},$$

where, now,

$$W = \lambda c R\{\tfrac{1}{2}(1 - \cos 2\alpha \cos 2\beta)\}^{\frac{1}{2}}$$
$$\sqrt{(M^2+N^2)} = \lambda c \sqrt{(\sin^2\alpha + \sin^2\beta)}.$$

It would probably be feasible to use a computer for the numerical evaluation of the right-hand side of the inequality above for all permissible values of α and β, and hence determine a suitable bound for λ given values of c, R, and D. However, a simplified version of the inequality may be obtained on the assumption that the critical values of α and β for stability differ very little from those appropriate to the case of no diffusion, i.e. $D = 0$. In this case, we have from the definitions of x and y,

$$\cos\alpha = \cos\beta = R$$

giving

$$W = \lambda c R^2 \sqrt{\{2(1-R^2)\}} \qquad \ldots (14)$$

and

$$\eta = R^2,$$

whence

$$\max C_i = \lambda c(1+R^2)\sqrt{\{2(1-R^2)\}}.$$

This yields

$$\lambda^2 \leqslant \frac{(1-D-R^4) + \{(1-D-R^4)^2 + D(2-D)\}^{\frac{1}{2}}}{4c^2(1-R^2)(1+R^2)^2} \qquad \ldots (15)$$

If the critical value of λ for $D = 0$ is denoted by λ_c, then

$$\lambda_c^2 = \frac{1}{2c^2(1+R^2)},$$

hence

$$\left(\frac{\lambda}{\lambda_c}\right)^2 \leqslant \frac{(1-D-R^4) + \{(1-D-R^4)^2 + D(2-D)\}^{\frac{1}{2}}}{2(1-R^4)}. \qquad \ldots (16)$$

If we neglect R^4 (max $R \approx \frac{1}{3}$), then

$$\left(\frac{\lambda}{\lambda_c}\right)^2 \leqslant 1 - \tfrac{1}{2}D.$$

Since
$$D = \frac{2K\delta t}{a^2}(\sin^2\alpha + \sin^2\beta) = \frac{2K\delta t}{a^2}(2 - 2R^2),$$
$$\left(\frac{\lambda}{\lambda_c}\right)^2 \leqslant 1 - \frac{2K\delta t}{a^2}(1 - R^2). \qquad \ldots (17)$$

K is chosen such that $K\delta t/a^2$ remains finite as a and $\delta t \to 0$.

It should be noted that this simplified treatment is possible only if diffusion is applied equally to all three variables, u, v, and h. If it is applied to u and v only, as is more usual, only two of the three diagonal elements of the matrix H are modified by the term D and the relationship between μ'_i and μ_i—the modified and unmodified eigenvalues—will be more complicated. It is reasonable to expect, however, that even in this case the approximate inequality for λ will provide useful guidance.

It is also necessary to consider the effect of incorporating a variable map factor in the governing equations of the 10-level model. The normal implication of this is that λ becomes equal to $m\delta t/a$ where a is the grid length at the North Pole. However, at the time of writing (November 1969) the map factor is not used in the diffusion term which thus remains simply

$$K\left(\frac{\partial^2 u}{\partial x^2} + \frac{\partial^2 u}{\partial y^2}\right)$$

etc., and *not*

$$Km^2\left(\frac{\partial^2 u}{\partial x^2} + \frac{\partial^2 u}{\partial y^2}\right).$$

This means that (17) is formally unaltered except that λ is now defined as $m\delta t/a$. Hence (17) can be written

$$\lambda^2 \leqslant \lambda_c^2\left\{1 - \frac{2K}{ma}(1 - R^2)\lambda\right\}$$

$$\text{or } \left\{\lambda + \frac{\lambda_c^2 K}{ma}(1 - R^2)\right\}^2 \leqslant \lambda_c^2 + \frac{\lambda_c^4 K^2}{m^2 a^2}(1 - R^2)^2,$$

$$\text{or } \lambda \leqslant -\frac{\lambda_c^2 K}{ma}(1 - R^2) + \lambda_c\left\{1 + \frac{\lambda_c^2 K^2}{m^2 a^2}(1 - R^2)^2\right\}^{\frac{1}{2}}. \qquad \ldots (18)$$

Example

Use of a diffusion coefficient of 10^7 m^2/s in the boundary zone of the small forecast area produced marked checker-board instability. An argument due to F. P. Bretherton shows that if ϵ is the percentage by which the critical time-step was violated we shall have a rate of growth of amplitude in N double time-steps of $(4\epsilon/100)^N$.

Examination of the results suggested that

$$(4\epsilon/100)^N = 10^4 \text{ for } N = 20,$$

whence $\epsilon \approx 40$. Since a time-step of $\delta t = 90$ s had been used, it seemed that the critical value of δt was about $(100 \times 90)/140 = 64{\cdot}5$ s.

If we use formula (18) with the values of m, λ_c, a, and R given below, we obtain a value for the critical time-step of 67·5 seconds.

Assumed values appropriate to the data under consideration were:

$c = 314$ m/s (corresponding to a surface temperature of 303K)

meteorological wind $V = 40$ m/s

$$\lambda_c^2 = \frac{1}{2(c^2 + v^2)} = 4{\cdot}9902 \times 10^{-6}\text{s}^2/\text{m}^2$$

$m = 1{\cdot}3201$ (corresponding to latitude 31°N)

$a = 5{\cdot}445 \times 10^4$m

$R = 40/314.$

Printed in England for Her Majesty's Stationery Office by J. W. Arrowsmith Ltd., Bristol 3 Dd501161 K8 12/70 3329

© *Crown copyright 1971*

Published by
HER MAJESTY'S STATIONERY OFFICE

To be purchased from
49 High Holborn, London WC1 6HB
13a Castle Street, Edinburgh EH2 3AR
109 St Mary Street, Cardiff CF1 1JW
Brazennose Street, Manchester M60 8AS
50 Fairfax Street, Bristol BS1 3DE
258 Broad Street, Birmingham 1
7 Linenhall Street, Belfast BT2 8AY
or through booksellers

SBN 11 400175 8